## Circulation

## ORIGINAL RESEARCH ARTICLE

## Metabolic Changes Associated With Cardiomyocyte Dedifferentiation Enable Adult Mammalian Cardiac Regeneration

Yuan-Yuan Cheng, PhD; Zachery Gregorich, PhD; Ray P. Prajnamitra, PhD; David J. Lundy, PhD; Ting-Yun Ma, BS; Yu-Hsuan Huang, BS; Yi-Chan Lee, MS; Shu-Chian Ruan, BS; Jen-Hao Lin, MS; Po-Ju Lin, MS; Chiung-Wen Kuo, PhD; Peilin Chen, PhD; Yu-Ting Yan, PhD; Rong Tian, MD, PhD; Timothy J. Kamp, MD, PhD; Patrick C.H. Hsieh, MD, PhD

**BACKGROUND:** Cardiac regeneration after injury is limited by the low proliferative capacity of adult mammalian cardiomyocytes (CMs). However, certain animals readily regenerate lost myocardium through a process involving dedifferentiation, which unlocks their proliferative capacities.

**METHODS:** We bred mice with inducible, CM-specific expression of the Yamanaka factors, enabling adult CM reprogramming and dedifferentiation in vivo.

**RESULTS:** Two days after induction, adult CMs presented a dedifferentiated phenotype and increased proliferation in vivo. Microarray analysis revealed that upregulation of ketogenesis was central to this process. Adeno-associated virus-driven HMGCS2 overexpression induced ketogenesis in adult CMs and recapitulated CM dedifferentiation and proliferation observed during partial reprogramming. This same phenomenon was found to occur after myocardial infarction, specifically in the border zone tissue, and HMGCS2 knockout mice showed impaired cardiac function and response to injury. Finally, we showed that exogenous HMGCS2 rescues cardiac function after ischemic injury.

**CONCLUSIONS:** Our data demonstrate the importance of HMGCS2-induced ketogenesis as a means to regulate metabolic response to CM injury, thus allowing cell dedifferentiation and proliferation as a regenerative response.

Key Words: cell dedifferentiation ■ cell proliferation ■ cellular reprogramming ■ HMGCS2 ■ ketogenesis

he adult human heart is incapable of replacing damaged or lost tissue because of the low proliferation rate of adult cardiomyocytes (CMs). Yet, certain animals, such as zebrafish, newts, and neonatal mice, exhibit robust regeneration of the myocardium after injury as a consequence of the dedifferentiation and proliferation of surviving CMs. A variety of approaches have been described to induce proliferation of adult CMs, including the delivery of growth factors or gene manipulation strategies, but robust and fully translational regeneration of the adult mammalian heart has not been achieved. In injured zebrafish hearts, some preexisting

CMs undergo dedifferentiation followed by proliferation, which allows complete cardiac regeneration. CM dedifferentiation is manifested by reactivation of embryonic cardiac gene expression and disassembly of contractile sarcomeres. The exact mechanisms responsible for triggering CM dedifferentiation are unknown. We hypothesized that if adult mammalian CMs were induced to dedifferentiate, this may enable CMs to initiate proliferation in response to relevant signals, thus allowing adult heart regeneration in mammals.

Metabolic flexibility is essential for the heart to adapt to various changes in the microenvironment, 13 and

Correspondence to: Patrick C.H. Hsieh, MD, PhD, Institute of Biomedical Sciences, Academia Sinica, Taipei 115, Taiwan. Email phsieh@ibms.sinica.edu.tw Supplemental Material is available at https://www.ahajournals.org/doi/suppl/10.1161/CIRCULATIONAHA.122.061960.

For Sources of Funding and Disclosures, see page 1966.

© 2022 American Heart Association, Inc.

Circulation is available at www.ahajournals.org/journal/circ

## **Clinical Perspective**

#### What Is New?

- · Temporary reprogramming of adult cardiomyocytes (CMs) in vivo results in dedifferentiation with changes in cell morphology, proliferation, and metabolism.
- · Upregulation of HMGCS2-mediated ketogenesis leads to a metabolic switch in the adult CMs during early reprogramming.
- · Loss of CM-specific HMGCS2 expression worsens heart function after cardiac ischemia/reperfusion injury, which can be rescued by exogenous HMGCS2 expression.

## What Are the Clinical Implications?

- Exploiting CM dedifferentiation and manipulating CM metabolism are potential mechanisms for cardiac regeneration after injury.
- HMGCS2 overexpression improves heart function after myocardial infarction and increases human induced pluripotent stem cell-derived CM dedifferentiation and proliferation under hypoxic conditions.

## Nonstandard Abbreviations and Acronyms

adeno-associated virus serotype 9 AAV9 cI/R cardiac ischemia/reperfusion

CM cardiomyocyte cTnT cardiac troponin T EF% ejection fraction percent

**EGFP** enhanced green fluorescent protein

FA fatty acid

**H3P** phosphohistone H3

hiPSC-CM human induced pluripotent stem cell-

derived cardiomyocyte

**iPSC** induced pluripotent stem cell

MI myocardial infarction

**NMR** nuclear magnetic resonance OCR oxygen consumption rate

ОНВ β-hydroxybutyrate

OSKM OCT4, SOX2, KLF4, and c-MYC

PPAR peroxisome proliferator-activated receptor

TEM transmission electron microscopy

WT wild type

changes in metabolism and substrate utilization are well demonstrated in CMs during development and after injury. Proliferative fetal CMs favor glycolysis to generate ATP during cardiac development; however, soon after birth, CMs begin to use primarily aerobic fatty acid (FA) metabolism. During the same time period, neonatal human CMs rapidly lose their proliferative ability,14 and

as the heart enlarges through childhood, rod-shaped CMs undergo hypertrophy rather than hyperplasia. When injured by hypoxic stress, CMs enlarge as a result of pathological hypertrophy, and their sarcomeric structures become disorganized. During this process, they also regain a small amount of proliferative ability, along with a metabolic switch to glycolysis. 15 This suggests that CM metabolism, dedifferentiation, and proliferation are intrinsically linked. Yet, in adult mammals, this adaptive response is not strong enough for complete cardiac regeneration after injury. Therefore, we hypothesized that exploring metabolic reprogramming may yield exploitable methods for inducing adult CM proliferation after injury.

ORIGINAL RESEARCH

As discovered by Dr Shinya Yamanaka, somatic cells can be reprogrammed by forced expression of OCT4, SOX2, KLF4, and c-MYC (OSKM) into induced pluripotent stem cells (iPSCs), which have characteristics similar to those of embryonic stem cells. 16 The reprogramming process involves several cellular changes, including the induction of proliferation, morphological alterations, and a metabolic switch. 17,18 Recently, shortterm expression of OSKM in adult CMs in vivo was shown to induce their dedifferentiation and reprogramming, enabling reentry of mammalian CMs into the cell cycle, thus facilitating heart regeneration.<sup>19</sup> These data support our hypothesis that reprogramming-induced dedifferentiation is a feasible strategy for promoting cardiac regeneration. However, the mechanisms underlying these changes have not been fully explored. In addition, reprogramming has limitations as a regeneration approach such as risk of tumorigenesis and loss of cellular epigenetic memory. Therefore, we aimed to identify potential downstream targets that may independently allow inducing adult CM dedifferentiation and enable proliferation. Here, we show that HMGCS2induced ketogenesis leads to metabolic switch in adult CMs during early reprogramming. This metabolic adaptation would increase adult CM dedifferentiation to facilitate cardiac regeneration after injury.

#### METHODS

All data and materials are available within the article. Detailed methods are described in the Supplemental Material.

## Animal Studies

All animal experiments were conducted in accordance with the Guide for the Use and Care of Laboratory Animals (Animal Research: Reporting of In Vivo Experiments guidelines), and all of the animal protocols have been approved by the experimental animal committee, Academia Sinica, Taiwan.

## **Data Availability**

Data sets are deposited and publicly available in the Gene Expression Omnibus database. The accession number is GSE169035.

## **Statistical Analysis**

The statistical data analyses were performed with GraphPad Prism, and data are shown as mean $\pm$ SEM. Unpaired Student t test and 2-way ANOVA were applied for statistical comparisons, and a value of  $P \le 0.05$  was considered significant.

## **RESULTS**

# In Vivo CM Reprogramming Induces Metabolic Switch, CM Dedifferentiation, and Increased CM Proliferation

To examine the process of adult CM reprogramming in vivo, transgenic mice were bred to overexpress mouse OSKM specifically in adult CMs after doxycycline induction, as shown in Figure 1A. Figure 1B and 1C show successful induction of OSKM mRNA and protein expression in isolated transgenic adult CMs after doxycycline treatment for 2 days. The substantial levels of OCT4 and SOX2 were detected without doxycycline treatment, indicating a certain leakiness of the genetic system in these CMspecific reprogramming mice. It is important to note that this high level of induction was detected mainly in CMs, not in non-CMs, in the heart or other tissues isolated from doxycycline-treated mice (Figure S1A). We noted an increase of Oct4 expression in the lung and kidney, which may contribute to the lethality of prolonged reprogramming induction in vivo. After tracking of the degree of CM proliferation, a 3-fold increase in BrdU+ CMs was found 2 days after doxycycline administration (Figure 1D and 1E). This proliferative response of adult CMs was highest at reprogramming day 2 compared with days 1 and 4. Gross heart function at reprogramming day 2 was measured by echocardiography and showed no difference in ejection fraction percent (EF%) (Figure 1F). Six days of doxycycline treatment was lethal. Examining the heart tissue after 5 days of doxycycline, we found more aggregated apoptotic cells (terminal deoxynucleotidyl transferase dUTP nick end labeling+ population) in reprogramming hearts compared with control hearts (Figure 1G). At the same time point, the mice had a significantly lower EF% by echocardiography (Figure 1H). Thus, we concluded that continuous induction of OSKM in adult CMs severely impairs heart function, leading to death. On this basis, reprogramming day 2 was selected as the key time point for our further analyses. Using intravital microscopy (Figure 1I) to investigate the isolated whole hearts with membrane potential dye (Di-2-ANEPEQ) staining, we found that CMs in control mice were normally aligned, but regions of poorly aligned CMs were observed in the doxycycline-treated mice (Figure 1J). In addition, the in vivo morphology of reprogramming CMs maintained the normal width but became shorter, leading to a rounder cell aspect ratio than control CMs (Figure 1K and 1L). By recording each contraction of the control or reprogramming hearts in vivo, we observed areas of disorganized or nonaligned contraction, consistent with the

structural disruptions (Figure S2). Furthermore, heart tissue sectioning was performed to examine the relationship between CM alignment (wheat germ agglutinin staining) and CM proliferation (Phosphohistone H3 staining). We confirmed that doxycycline-induced hearts contained more proliferative CMs and that these same cells displayed a rounder morphology (≈50-60 µm in length and an aspect ratio of ≈3) with poorer cell alignment (Figure 1M-10). Finally, CMs were isolated from the hearts of mice treated for 2 days with PBS or doxycycline, and RNA was extracted and subjected to microarray analysis (Figure 1P). Gene ontology categorization showed that metabolism-related gene expression was significantly changed in the reprogramming CMs compared with the control CMs at reprogramming day 2 (Figure 1Q). The gene expression changes included the upregulation of glucose and amino acid metabolism and the downregulation of nucleotide metabolism. Similar trends were shown in heat map analysis (Figure 1R); ketone metabolism-related gene expression was upregulated, and aerobic respiration-related genes were downregulated in the adult reprogramming CMs compared with the control CMs. Taken together, these data show that temporary CM reprogramming resulted in dedifferentiation, with changes in cell morphology, proliferation, and expression of genes associated with metabolism.

## Cardiac-Specific Ketogenesis Creates a Systemic and Specific Metabolic Switch, Along With Mitochondrial Changes, Inducing CM Dedifferentiation at Reprogramming Day 2

Because a metabolic switch appears to be implicated in adult CM dedifferentiation, we decided to clarify any rearrangement of metabolic pathways in adult CMs during the reprogramming process. First, the metabolites of control and CM-reprogramming heart lysates were analyzed by liquid chromatography-mass spectrometry, identifying 101 metabolites in both groups (Figure 2A and 2B). Grouping these hits revealed that glucose and ketone body metabolism-related metabolites were upregulated in CM-reprogramming hearts (Figure 2C), in agreement with gene expression changes identified by microarray. On the contrary, tricarboxylic acid cycle and nucleotide metabolism-related metabolites were downregulated in CM-reprogramming hearts (Figures 1R and 2C). To avoid influence by intermediate products derived from other tissues, an ex vivo heart system was set up, and carbon nuclear magnetic resonance (NMR) was used to detect the <sup>13</sup>C-metabolites produced only from the exogenous addition of labeled substrates (Figure 2D).20 In NMR analysis, mixed FAs, which are the primary fuel for adult cardiac aerobic respiration, were decreased in the reprogramming hearts compared with the control hearts (Figure 2E). Although glucose and ketones slightly increased for ATP generation, the total percentage of aerobic respiration, derived from perfused

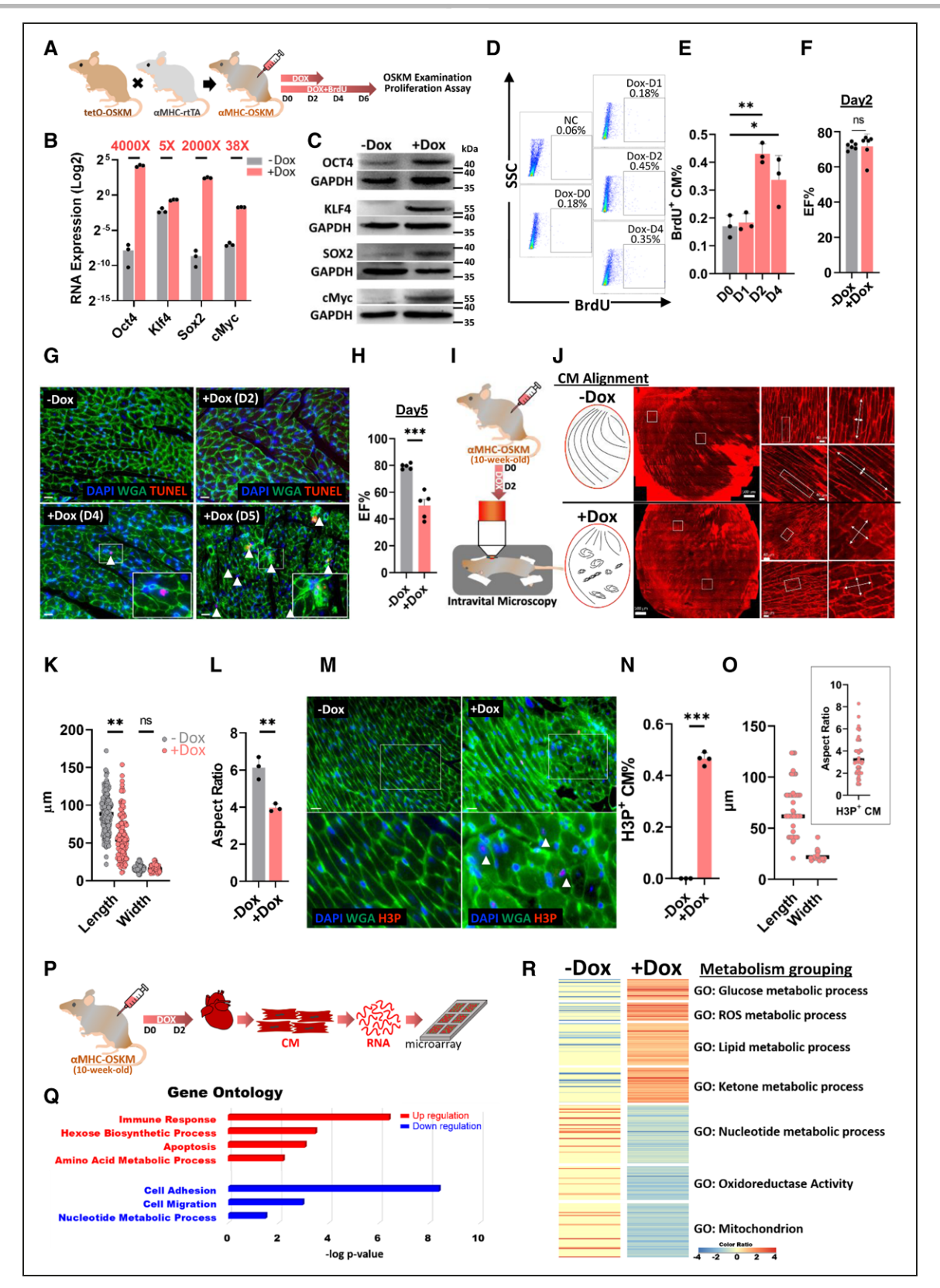


Figure 1. In vivo CM reprogramming induces metabolic switch, CM dedifferentiation, and increased CM proliferation. A, Experimental design for investigating adult cardiomyocyte (CM) reprogramming in vivo. B, RNA expression level and induction level of Oct4, Sox2, KIf4, and c-Myc (OSKM) in adult CMs after induction of OSKM reprogramming for 2 days. C, Protein expression level and induction level of OSKM in adult CMs after induction of OSKM reprogramming for 2 days. D, Flow cytometry analysis of isolated proliferative CMs through BrdU tracking in CM-reprogramming mice after OSKM induction. **E**, Percentage of proliferative CMs at each CM-reprogramming day determined by flow cytometry. F, Heart function measured by echocardiography in control or CM-reprogramming hearts after (Continued)

Figure 1 Continued. doxycycline treatment for 2 days. G, Terminal deoxynucleotidyl transferase dUTP nick end labeling (TUNEL) staining of heart sections isolated from CM-OSKM mice after doxycycline treatment at the different time points. H, Heart function measured by echocardiography in control or CM-reprogramming hearts after doxycycline treatment for 5 days. I, Schematic diagram of intravital imaging protocol used for live investigating of CM-reprogramming hearts after PBS or OSKM induction in vivo for 2 days. J, Investigation of CM alignment in the whole CM-reprogramming hearts by intravital microscopy after PBS or OSKM induction in vivo for 2 days. K, Morphology of CMs in CM-reprogramming hearts determined by length and width in intravital imaging data after PBS or OSKM induction in vivo for 2 days. Each dot represents 1 CM in 1 control or reprogramming heart. L, Aspect ratio determined by length-to-width ratio of each CM-reprogramming mouse in intravital imaging data after PBS or OSKM induction specifically in CMs in vivo for 2 days. Each dot represents 1 mouse sample. M, Immunofluorescence staining of heart tissue sections showing morphology of proliferative CMs through Phosphohistone H3 (H3P) and wheat germ agglutinin (WGA) staining on CM-reprogramming hearts after PBS or OSKM induction for 2 days. Arrowheads indicate H3P+ proliferative CMs. Scale bars are 50 µm. N, Percentage of proliferative CM percentage (H3P+ CM%) in the heart tissue sections of CM-reprogramming hearts after PBS or OSKM induction for 2 days. O, Morphology of H3P+ CMs in 3 CM-reprogramming hearts determined by length, width, and aspect ratio in heart tissue sections after OSKM induction in vivo for 2 days. Each dot represents 1 CM in 1 control or reprogramming heart. P, Experimental design for discovering the detailed mechanism for adult CM reprogramming at day 2 by microarray analysis. Q, Gene ontology (GO) analysis of gene expressional changes in adult CMs after PBS or OSKM induction for 2 days in vivo. R, Heat map showing metabolism-related gene expressional changes in adult CMs after PBS or OSKM induction for 2 days in vivo.

<sup>13</sup>C metabolites, was decreased in the reprogramming hearts (Figure 2E and Figure S4). In addition, the amounts of lactate and alanine were 1.5 times higher in reprogramming hearts than in control hearts, indicating that glycolysis was increased in the hearts 2 days after OSKM induction (Figure 2F). An interesting finding was that  $\beta$ -hydroxybutyrate (OHB) was 2 times higher in the reprogramming hearts than in the control hearts, indicating that ketogenesis is increased (Figure 2F). Several techniques were further used to confirm ketogenesis induction (Figure 2G). The main intermediate product of ketogenesis is 3-hydroxy-3-methylglutaryl-CoA. Therefore, we isolated mitochondria and confirmed that the 3-hydroxy-3-methylglutaryl-CoA amount was 2 times higher in the reprogramming hearts than in the control hearts (Figure 2H). The end product of ketogenesis, OHB, was measured at >1.5 times higher in the reprogramming CMs than control CMs by an OHB colorimetric assay kit (Figure 2I). To control for potential metabolic effects of doxycycline, we performed the same metabolic profiling on C57BL/6J (normal) mice treated with doxycycline for 2 days. The levels of each <sup>13</sup>C-metabolite were unchanged in doxycycline-treated normal hearts compared with PBS-treated CM-OSKM mice (Figure S5A). In addition, neither HMGCS2 expression nor OHB levels were significantly different (Figure S5B and S5C). Using seahorse assay, we found that the oxygen consumption rate (OCR) was lower in the adult reprogramming CMs than in the control CMs (Figure 2J and 2K). HMGCS2, the rate-limiting enzyme of ketogenesis, was significantly increased at both the RNA and protein levels (Figure 2L and 2M). A schematic summary of these changes is shown in Figure 2N. Several metabolic pathways such as ketogenesis and aerobic respiration occur in mitochondria, and changes of OCR are often accompanied by mitochondrial differences. Therefore, we assessed CM mitochondria presenting that mitochondrial copy numbers were lower and RNA expression was significantly lower in the reprogramming CMs compared with the control CMs (Figure 20 and 2P). Transmission electron microscopy (TEM) revealed that mitochondrial area and aspect ratio were both significantly decreased

in the reprogramming hearts (Figure 2Q–2S). Mitochondrial fission has been reported to be related to proliferative induction through posttranslational phosphorylation of DRP-1 on serine 616.21 Indeed, DRP-1 serine 616 phosphorylation was higher in reprogramming CMs compared with control CMs (Figure S6A), whereas DRP-1 on serine 637 showed no difference (Figure S6B). In summary, these data indicate that during CM reprogramming by OSKM induction, a metabolic switch occurs, including increased ketogenesis and glycolysis, with deceased aerobic respiration and altered mitochondrial structure and function. This switch occurs in synchrony with the induction of CM proliferation.

## HMGCS2 Induction in Adult Hearts Induces Ketogenesis, Leading to a Metabolic Switch in an Oxygen-Dependent Manner

We decided to examine whether ketogenesis is the initiator of these metabolic changes in the heart. In vivo overexpression of HMGCS2 in normal adult mouse hearts was established through adeno-associated virus serotype 9 (AAV9) infection to test whether its overexpression would lead to the same metabolic changes found in reprogramming hearts (Figure 3A). AAV9-mediated HMGCS2 induction was sustained for ≈2 months, and the expression peaked 5 weeks after injection (Figure S7A). Transduction efficiency was ≈88% by measuring EGFP+ (enhanced green fluorescent protein-positive) cells with flow cytometry (Figure S7B). After AAV9 infection for 5 weeks, both HMGCS2 expression and the amount of OHB were confirmed to be increased in the isolated adult CMs from AAV9-HMGCS2 mice compared with AAV9-EGFP (control) mice (Figure 3B and 3C). Metabolic profiles of control and HMGCS2overexpressing hearts were analyzed to determine that ketogenesis was induced and aerobic FA metabolism was decreased in the HMGCS2-overexpressing hearts (Figure 3D and 3E). This was in agreement with what we observed in the OSKM-induced adult CMs. However, under normal oxygen conditions, energy demand could be supplied from aerobic glucose and OHB metabolism

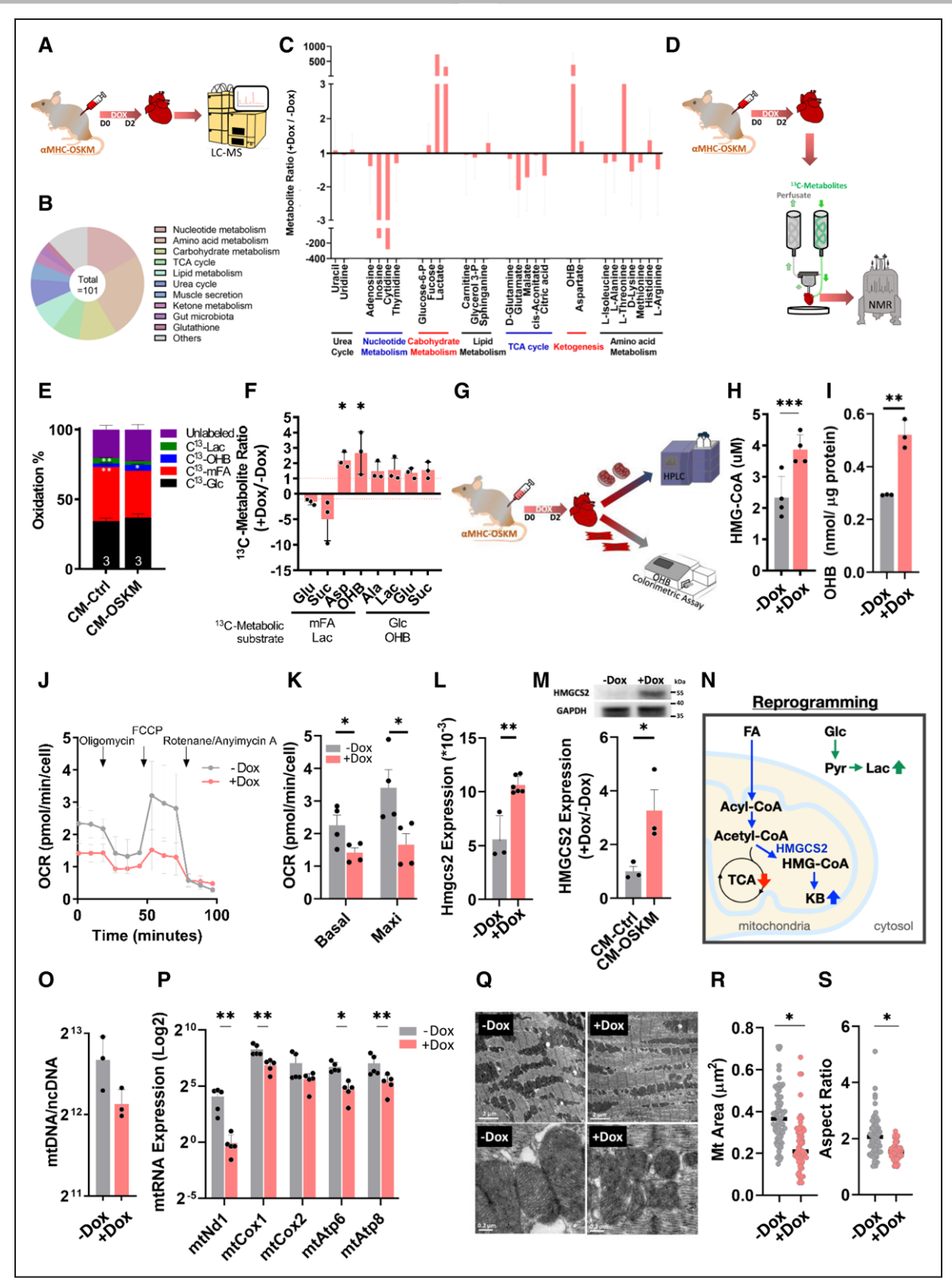


Figure 2. Cardiac-specific ketogenesis creates a systemic and specific metabolic switch along with mitochondrial changes, inducing CM dedifferentiation at reprogramming day 2.

A, Experimental design for metabolic profiling using liquid chromatography-mass spectrometry (LC-MS) analysis. B, Hits detected by LC-MS analysis especially in both control and cardiomyocyte (CM)-reprogramming hearts. C, Grouping of metabolic hits detected by LC-MS analysis in control or CM-reprogramming hearts. D, Experimental design for metabolic profiling using a working heart system perfused with 13C-metabolites, detected by nuclear magnetic resonance (NMR). E, Oxidation percentage of control and CM-reprogramming hearts measured by 13C-glutamate level derived from different <sup>13</sup>C-metabolic substrates through NMR analysis. **F**, Specific <sup>13</sup>C-metabolites of control and (*Continued*)

Figure 2 Continued. CM-reprogramming hearts detected by NMR. **G**, Experimental design for measuring ketogenesis in control or CM-reprogramming hearts. **H**, HMG-CoA level detected by high-performance liquid chromatography in the isolated mitochondria from control or CM-reprogramming hearts. **I**, β-Hydroxybutyrate (OHB) level measured by OHB colorimetric assay in the isolated CMs from control or CM-reprogramming mice. **J**, Oxygen consumption rate (OCR) detected by seahorse analysis in isolated CMs from control or CM-reprogramming mice. **K**, Quantification of basal and maximal OCRs in the control or reprogramming CMs isolated from PBS- or OCT4, SOX2, KLF4, and c-MYC (OSKM)-treated hearts. **L**, RNA expression of Hmgcs2 normalized by Gapdh in CMs isolated from control or OSKM-treated mice. **M**, Protein expression of HMGCS2 in CMs isolated from control (Ctrl) or OSKM-treated mice. **N**, Schematic diagram showing metabolic switch in adult CMs after OSKM induction for 2 days. **O**, Mitochondrial copy numbers detected by mtDNA through real-time polymerase chain reaction (PCR) in control or reprogramming CMs isolated from PBS or OSKM-treated hearts. **P**, Mitochondrial RNA expression detected by real-time PCR in control or reprogramming CMs isolated from PBS- or OSKM-treated hearts. These RNA expressions were normalized by Gapdh. **Q**, Mitochondrial structure examined by transmission electron microscopy (TEM) in isolated control or CM-reprogramming hearts. **R**, Mitochondrial (Mt) size in isolated control or CM-reprogramming hearts, determined by TEM. **S**, Aspect ratio of mitochondrial length-to-width in isolated control or CM-reprogramming, determined by TEM. TCA indicates tricarboxylic acid.

(Figure 3D and 3E). Glycolysis was also increased, likely to compensate for decreased ATP production through aerobic FA metabolism (Figure 3E). Seahorse analysis showed that OCR was not different in HMGCS2-overexpressing CMs compared with controls (Figure 3F and 3G). In accordance with the finding that the total oxidation rate was not changed in the HMGCS2-overexpressing hearts, mitochondrial DNA and RNA expression, as well as mitochondrial structure, did not differ between control and HMGCS2-overexpressing hearts (Figure S8A-S8E). In addition, heart function was similar between control and HMGCS2-overexpressing hearts. Therefore, we conclude that cardiac HMGCS2 overexpression increases ketogenesis, which, in turn, decreases aerobic FA metabolism and increases glycolysis and aerobic glucose metabolism, together maintaining oxygen consumption and overall energy production (Figure 3H). Although cardiac ketogenesis competitively reducing aerobic FA metabolism was shown in reprogramming hearts and cardiac HMGCS2-overexpressing hearts, the following metabolic outcome would differ according to environmental adaptation (Figures 2N and 3H). This implies that cardiac ketogenesis may lead to a "reprogramming metabolism," allowing adult CM dedifferentiation under temporary induction of Yamanaka factors. To test this hypothesis, cardiac HMGCS2 overexpression was performed on adult CM-OSKM mice to confirm whether this overexpression would increase CM proliferative ability while inducing reprogramming. First, we examined the morphology of highly HMGCS2-expressing CMs from CM-OSKM mice after OSKM induction for 2 days. These cells displayed a rounder morphology (50–60 µm in length and aspect ratio of ≈3) similar to those we found in reprogramming CMs (Figure 3I and 3J). After HMGCS2 overexpression resulting from doxycycline treatment, the hearts showed ≈2-fold higher *Hmgcs2* RNA expression compared with the doxycycline treatment only or HMGCS2 overexpression only (Figure 3K). Through BrdU labeling of isolated adult CMs, flow cytometric analysis showed a 2-fold increased BrdU+ population compared with the control reprogramming hearts (Figure 3L and 3M). Heart tissue sectioning was also performed and showed 2-fold increase in the H3P+ CM population in HMGCS2-overexpressing reprogramming

hearts compared with the control reprogramming hearts (Figure 3N and 30). These proliferative cells were also confirmed as HMGCS2+ CMs (Figure S9). However, the discrepancy of lower H3P+ CM population detected in the AAV9-EGFP group than the +doxycycline group shown in Figure 1M may be attributable to the different mouse strains we used for AAV injection. Furthermore, the reprogramming-induced CMs were isolated for in vitro culture and showed 3 times more H3P+/ cardiac troponin T (cTnT)+ CMs in HMGCS2-overexpressing reprogramming hearts compared with the control reprogramming hearts (Figure 3P and 3Q). To further investigate whether HMGCS2 is necessary for the proproliferative effects of OSKM expression, trigenic mice with CM-specific doxycycline-inducible OSKM expression in HMGCS2+/- mice were bred. After 2 days of doxycycline and BrdU administration, adult CMs isolated from HMGCS2 heterozygous mutant CMs had a 2.5 times lower BrdU+ CM percentage than control CMs (Figure S10A and S10B). In addition, adult CMs were isolated for in vitro culture, and the proliferative H3P+/ cTnT+ CM percentage was 3.5 times lower in HMGCS2 heterozygous mutant mice compared with control mice. These proliferative CMs showed a rounder morphology than the nonproliferative CMs (Figure S10C and S10D). In conclusion, the results in Figure 3 show that HMGCS2 overexpression by itself induces ketogenesis but does not trigger proliferation of CMs. However, in CM-OSKM-induced hearts, HMGCS2 overexpression enhanced proliferation compared with controls.

## CM-Specific HMGCS2 Knockout Mice Present a Metabolic Switch, Along With Impaired Mitochondria, Leading to a Pathological Hypertrophy

CM-specific HMGCS2 knockout mice were established to investigate the effects on cardiac metabolism. Conditional HMGCS2 knockout mice (floxP-HMGCS2) were bred by inserting loxP sites flanking exon 2 of HMGCS2 in the genome (Figure 4A). Through cross-breeding with  $\alpha$ -myosin heavy chain promoter-driven CRE mice, CM-specific knockout mice (CM-HMGCS2 $^{-/-}$ ) were established (Figure S11A). These mice showed loss

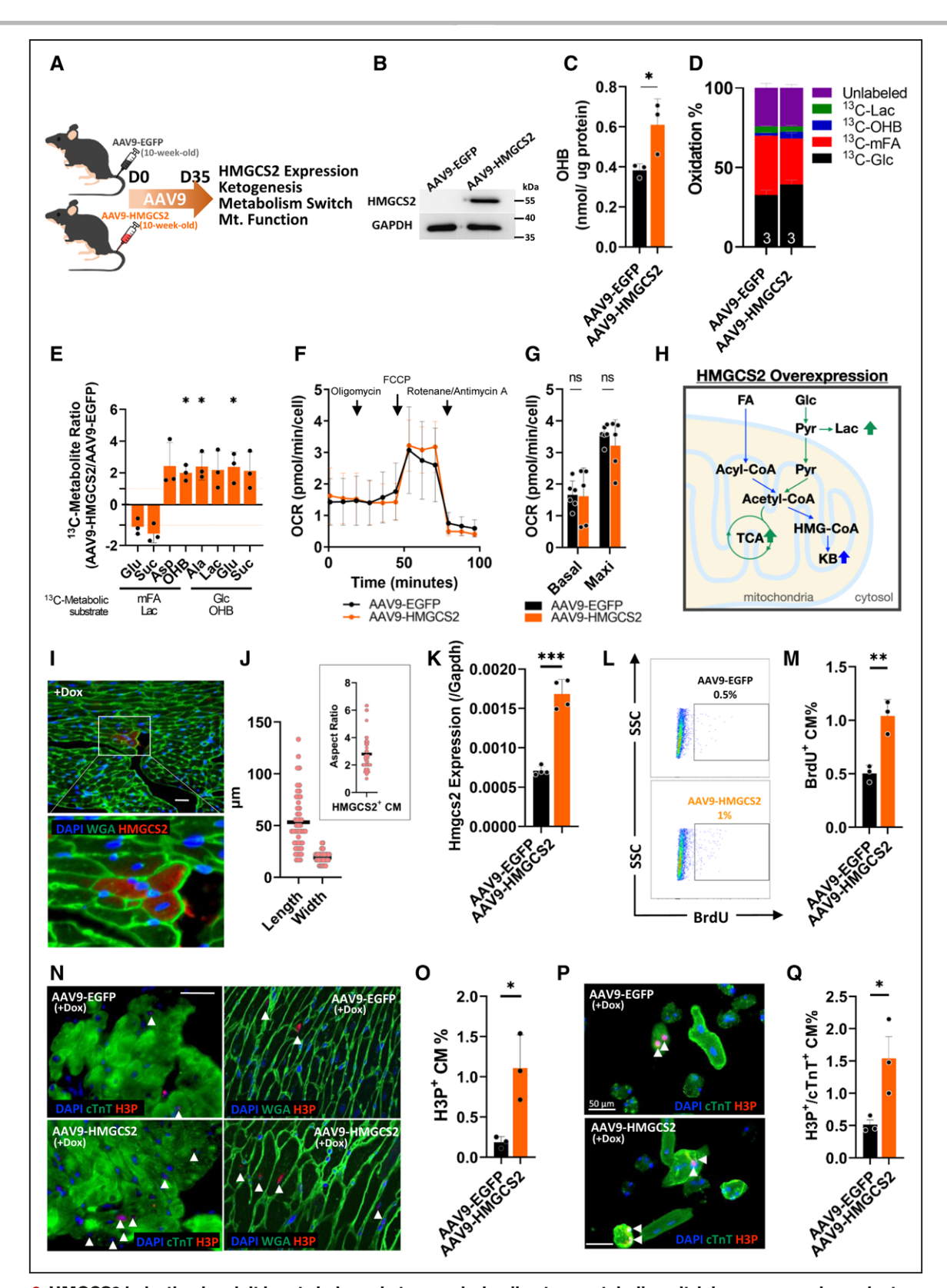


Figure 3. HMGCS2 induction in adult hearts induces ketogenesis, leading to a metabolic switch in an oxygen-dependent manner. A, Experimental design for HMGCS2 overexpression in vivo through adeno-associated virus serotype 9 (AAV9) infection. B, Protein expression of HMGCS2 detected by Western blot in AAV9-EGFP (enhanced green fluorescent protein) or AAV9-HMGCS2-infected CMs. C, β-Hydroxybutyrate (OHB) level measured by colorimetric assay in the isolated cardiomyocytes (CMs) from AAV9-EGFP- or AAV9-HMGCS2infected hearts. D, Oxidation percentage of AAV9-EGFP- or AAV9-HMGCS2-infected hearts measured by 13C-glutamate level derived from different <sup>13</sup>C-metabolic substrates though nuclear magnetic resonance (NMR) analysis. **E**, Specific <sup>13</sup>C-metabolites of (Continued)

Figure 3 Continued. AAV9-EGFP- or AAV9-HMGCS2-infected hearts detected by NMR. F, Oxygen consumption rate (OCR) detected by seahorse analysis in the isolated CMs from AAV9-EGFP- or AAV9-HMGCS2-infected mice. G, Quantification of basal and maximal OCRs in the AAV9-EGFP- or AAV9-HMGCS2-infected CMs. H, Representative diagram of metabolic switch in adult CMs after AAV9-EGFP or AAV9-HMGCS2 infection. I, Immunofluorescence staining of heart tissue sections showing morphology of highly HMGCS2-expressing CMs through HMGCS2 and wheat germ agglutinin (WGA) staining on CM-reprogramming hearts after OCT4, SOX2, KLF4, and c-MYC (OSKM) induction for 2 days. Scale bar was 50 μm. J, Morphology of highly HMGCS2-expressing CMs in 3 CM-reprogramming hearts determined by length, width, and aspect ratio in the heart tissue sections after OSKM induction in vivo for 2 days. Each dot represents 1 CM in 3 reprogramming hearts. K, RNA expression of Hmgcs2 normalized by Gapdh in CMs isolated from control or OSKM-treated mice after HMGCS2 overexpression. L, Percentage of isolated proliferative CM measured by flow cytometry through BrdU tracking in control or HMGCS2 overexpressed CM-reprogramming mice. M, Statistics of flow cytometric data representing the percentage of proliferative CMs in control or HMGCS2-overexpressed CM-reprogramming mice. N, Immunofluorescence of heart tissue sections to present morphology of proliferative CMs through H3P and WGA staining on control or HMGCS2-overexpressed CM-reprogramming hearts. Arrowheads indicate H3P+ proliferative CMs. Scale bar was 50 μm. **0**, Quantification of proliferative CM percentage (H3P+ CM%) in the heart tissue sections of control or HMGCS2-overexpressed CM-reprogramming hearts. P, Immunofluorescence of isolated CMs showing morphology of proliferative CMs through H3P and cardiac troponin T (cTnT) staining from control or HMGCS2-overexpressed CM-reprogramming hearts. Scale bar was 50 μm. Q, Proliferative CM percentage (H3P+/cTnT+ CM%) in the isolated CMs from control or HMGCS2-overexpressed CM-reprogramming hearts. TCA, tricarboxylic acid.

of HMGCS2 RNA and protein expression in isolated CMs even when we loaded more total protein (40 μg; Figure 4B). OHB was undetectable in adult CM-HMGCS2<sup>-/-</sup> CMs (Figure 4C). Cardiac function was then measured by echocardiography and catheterization. EF% was significantly decreased in the CM-HMGCS2<sup>-/-</sup> mice (Figure 4D), and left ventricular pressure-volume indices revealed impaired heart function in the knockout mice compared with the control mice (Figure S11B). The dP/dt values were higher in CM-HMGCS2+/+ mice compared with CM-HMGCS2<sup>-/-</sup> mice under basal conditions (Figure S11B). During occlusion, CM-HMGCS2+/+ hearts showed higher end-systolic pressure-volume relationship, end-diastolic pressure-volume relationship, and preload recruitable stroke work values and lower tau values than HMGCS2-/- hearts (Figure S10B). The left ventricular mass was found to be higher in the CM-HMGCS2<sup>-/-</sup> mice compared with control mice (Figure 4E). The hypertrophic marker by the ratio of  $\beta$ myosin heavy chain to  $\alpha$ -myosin heavy chain expression was increased 2-fold in the CM-HMGCS2-/- mice (Figure 4F), whereas PGC1 $\alpha$  expression was not changed, indicating the presence of pathological hypertrophy in the CM-HMGCS2-/- mice (Figure 4G). Through trichrome staining of adult mouse heart tissue sections, both the percentage of fibrotic areas and CM size were significantly increased in the CM-HMGCS2-/- mice compared with the CM-HMGCS2+/+ mice (Figure 4H-4J). Gradual decreases of HMGCS2 expression were detected, with embryonic hearts showing much higher HMGCS2 expression than adult hearts (Figure S11C). In addition, the proliferative ability of CMs isolated from newborn CM-HMGCS2-/- mice was examined, showing a significantly lower H3P+ and AURKB+ CM% compared with the control mice (Figure 4K-4N). After the mice reached adulthood, the number of rod-shaped CMs in CM-HMGCS2<sup>-/-</sup> mice was reduced by approximately half compared with control mice (Figure S11D). Thus, we hypothesize that CM-HMGCS2<sup>-/-</sup> mice generated fewer total CMs during development and that hypertrophy may be used as a compensatory mechanism to maintain sufficient heart growth during adolescence. The metabolic

profile of adult CM-HMGCS2-/- hearts was analyzed, revealing that glucose became the principal substrate for aerobic respiration (Figure S11E) and that glycolysis also increased, as shown by increased lactate (Figure S11F). Ketogenesis was also reduced, as shown by decreased OHB (Figure S10F). The OCR was also measured and found to be significantly decreased in CMs isolated from CM-HMGCS2<sup>-/-</sup> mice (Figure 40 and 4P). Accordingly, total mitochondrial DNA copies and the RNA expression of key mitochondrial genes were lower than in CM-HMGCS2<sup>+/+</sup> mice (Figure 4Q and 4R). TEM was used to find both misalignment and altered mitochondrial size and aspect ratio of CM-HMGCS2<sup>-/-</sup> mice compared with CM-HMGCS2+/+ mice (Figure 4S-4U). These data indicate that a reduction of HMGCS2 expression in the CMs leads to the rearrangement of metabolic pathways, along with impaired mitochondria, resulting in pathological hypertrophy and damaged heart function.

## Loss of CM-Specific HMGCS2 Expression Worsens Heart Function After Cardiac Ischemia/Reperfusion Injury and Can Be Rescued by Exogenous HMGCS2 Expression

Although HMGCS2 expression is low in the adult heart, its role in development and maintenance of heart function is clearly shown in Figure 4. Next, we decided to investigate any role of HMGCS2 in cardiac protection or regeneration because injured hearts may create an environment similar to that of OSKM-induced reprogramming hearts. Both hearts showed significant upregulation of dedifferentiation markers Myh7 and Nkx2.5 (Figure S12A), and Hmgcs2 was highly upregulated in CMs after the induction of OSKM in adult CM of mice with myocardial infarction (MI; Figure S12B). In addition, HMGCS2 expression was reported to be directly regulated by MYC protein.<sup>22</sup> CM-HMGCS2<sup>-/-</sup> mice displayed impaired heart function even without cardiac injury (Figure 4). However, CM-HMGCS2+/mice, confirmed to have half the amount of HMGCS2 expression, still produced OHB equal to the control

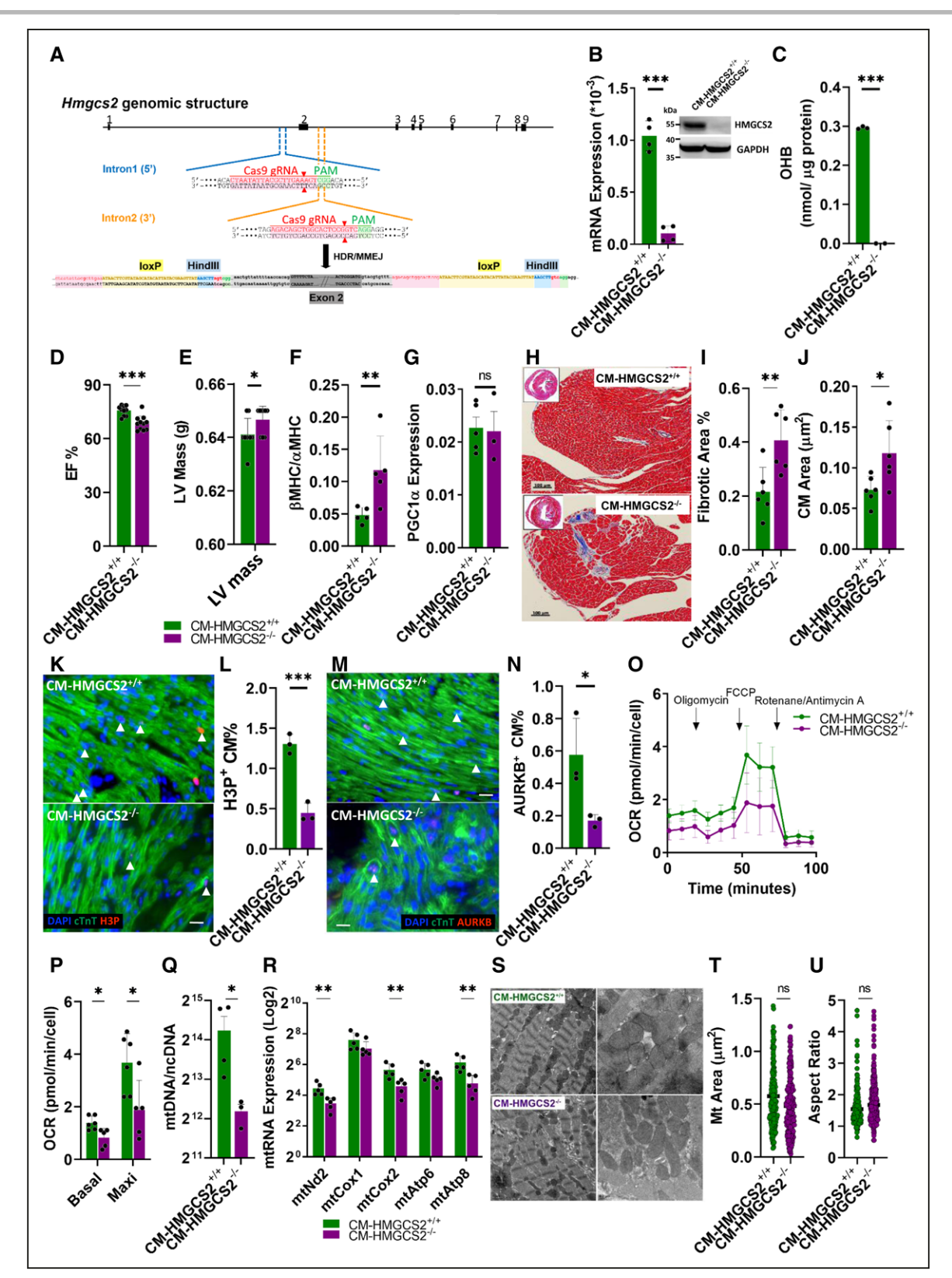


Figure 4. CM-specific HMGCS2 knockout mice present a metabolic switch along with impaired mitochondria leading to a pathological hypertrophy.

A, Schematic diagram showing establishment of cardiomyocyte (CM)-specific HMGCS2 knockout mice. B, RNA and protein expression of HMGCS2 detected by real-time polymerase chain reaction (PCR) and Western blot in isolated CMs from 10-week-old CM-HMGCS2+/+ or CM-HMGCS2<sup>-/-</sup> mice. Protein (40 μg) was loaded for examination. RNA expression was normalized by Gapdh. **C**, β-Hydroxybutyrate (OHB) level measured by OHB colorimetric assay in isolated CMs from 10-week-old CM-HMGCS2+/+ or CM-HMGCS2-/- mice. (Continued)

Figure 4 Continued. D, Ejection fraction percent (EF%) of 10-week-old CM-HMGCS2+/+ or CM-HMGCS2-/- hearts measured by echocardiography. **E**, Left ventricular (LV) mass of 10-week-old CM-HMGCS2+/+ or CM-HMGCS2-/- hearts measured by echocardiography. F, RNA expression of hypertrophic markers β-myosin heavy chain (MHC) and αMHC measured by real-time PCR in the isolated CMs from 10-week-old CM-HMGCS2+/+ or CM-HMGCS2-/- mice. RNA expression was normalized by Gapdh. **G**, RNA expression of PGC1 $\alpha$  measured by real-time PCR in the isolated CMs from 10-week-old CM-HMGCS2+/+ or CM-HMGCS2-/- mice. H, Fibrotic area in 10-week-old CM-HMGCS2+/+ or CM-HMGCS2-/- hearts shown by Masson trichrome staining of heart tissue sections. I, Quantification of fibrotic percentage in 10-week-old CM-HMGCS2+/+ or CM-HMGCS2-/- hearts measured by Masson trichrome staining. J, Quantification of CM size in 10-weekold CM-HMGCS2+/+ or CM-HMGCS2-/- hearts measured by Masson trichrome staining. K, Immunofluorescence of heart tissue sections to present morphology of proliferative CMs through H3P and cardiac troponin T (cTnT) staining on 1-day-old control or CM-HMGCS2<sup>-/-</sup> hearts. Arrowheads indicate H3P+/cTnT+ proliferative CMs. Scale bars are 50 µm. L, Quantification of proliferative CM percentage (H3P+ CM%) in the heart tissue sections of 1-day-old control or CM-HMGCS2-/- hearts. M, Immunofluorescence of heart tissue sections showing morphology of proliferative CMs through AURKB and cTnT staining on 1-day-old control or CM-HMGCS2-/- hearts. Arrowheads represent AURKB+/ cTnT+ proliferative CMs. Scale bars are 50 µm. N, Statistics of proliferative CM percentage (AURKB+ CM%) in the heart tissue sections of 1-day-old control or CM-HMGCS2-/- hearts. O, Oxygen consumption rate (OCR) detected by seahorse analysis in the isolated CMs from CM-HMGCS2+/+ or CM-HMGCS2-/- mice. P, Quantification of basal and maximal OCRs in the isolated CMs from 10-week-old CM-HMGCS2+/+ or CM-HMGCS2-/- mice. Q, Mitochondrial copy numbers detected by mtDNA through real-time PCR in the isolated CMs from 10-week-old CM-HMGCS2+/+ or CM-HMGCS2-/- mice. R, Mitochondrial RNA expression detected by real-time PCR in adult CMs isolated from 10-week-old  $CM-HMGCS2^{+/+} \ or \ CM-HMGCS2^{-/-} \ mice. \ RNA \ expressions \ were \ normalized \ by \ Gapdh. \ \textbf{S}, \ Mitochondrial \ structure \ examined \ by \ transmission$ electron microscopy (TEM) in 10-week-old CM-HMGCS2+/+ or CM-HMGCS2-/- hearts. T, Mitochondrial size of isolated 10-week-old CM-HMGCS2+/+ or CM-HMGCS2-/- hearts in TEM data. U, Aspect ratio of mitochondrial length-to-width in isolated 10-week-old CM-HMGCS2+/+ or CM-HMGCS2-/- hearts in TEM data.

mice and maintained normal heart function (Figure S13A-S13C). Therefore, HMGCS2+/- mice were used to investigate the role of HMGCS2 in cardiac regeneration after cardiac ischemia/reperfusion (cl/R) injury (Figure 5A). Both HMGCS2 expression and OHB were significantly lower in the CM-HMGCS2+/- mice 1 day after cl/R surgery (Figure 5B and 5C), which was the peak of HMGCS2 upregulation in CM-HMGCS2<sup>+/+</sup> mice (Figure S12C). One day after cl/R, CM-HMGCS2+/- mice showed a significantly larger infarct area percentage than CM-HMGCS2+/+ mice (Figure 5D and 5E). EF% was reduced in both CM-HMGCS2+/+ and CM-HMGCS2+/- mice 1 day after cl/R injury. Weekly analysis revealed that EF% slightly decreased over time in CM-HMGCS2+/- mice, whereas CM-HMGCS2+/+ mice showed a small increase in EF% because of to innate recovery. At day 21, this difference was statistically significant (Figure 5F). Heart function was further characterized by catheterization at postinjury day 21, and all indices indicated poorer heart function in CM-HMGCS2+/- mice than CM-HMGCS2<sup>+/+</sup> mice (Figure 5G). The percentage of fibrotic area was also higher in the CM-HMGCS2+/mice compared with the CM-HMGCS2+/+ mice at day 21 after cl/R (Figure 5H and 5l). Next, we examined whether exogenous induction of HMGCS2 expression into CM-HMGCS2+/- mice may rescue cardiac function after cI/R injury. After exogenous HMGCS2 induction by AAV9 for 5 weeks, HMGCS2 expression and OHB amount were both highly upregulated in HMGCS2-rescued CM-HMGCS2+/- mice compared with control mice 1 day after cI/R injury (Figure 5J and 5K). HMGCS2-rescued CM-HMGCS2+/- mice showed a lower infarct area percentage than control CM-HMGCS2+/- mice (Figure 5L and 5M). Echocardiography revealed that heart function was also rescued, showing higher EF% at day 21 after cI/R surgery in the HMGCS2-rescued mice (Figure 5N). Catheter

measurements indicated a trend toward improved systolic and diastolic functions in HMGCS2-rescued mice after cI/R injury for 21 days compared with control mice (Figure 50). At the same time, the percentage of fibrotic area was lower in HMGCS2-rescued mice compared with control mice (Figure 5P and 5Q).

According to the results shown in Figures 2 and 3, cardiac ketogenesis should competitively reduce aerobic FA metabolism, leading to a metabolic switch based on oxygen level. This implies that HMGCS2induced metabolic changes should be different in the hypoxic infarct area versus the normoxic remote area of hearts after cI/R injury. To test this hypothesis, heart tissue from each area was isolated and perfused with <sup>13</sup>C-glucose through a working heart system. NMR data revealed that the ratio of <sup>13</sup>C-lactate to <sup>13</sup>C-succinate (glycolysis/aerobic glucose metabolism) was significantly higher in the infarct area of HMGCS2-rescued hearts (Figure 5R and Figure S14A and S14B). This indicates that a higher rate of adult CM glycolysis in the border zone would induce their dedifferentiation, allowing proliferation, which we previously found during CM reprogramming (Figure 2N). However, the <sup>13</sup>C-lactate to <sup>13</sup>C-succinate ratio was lower, and both <sup>13</sup>C-lactate and <sup>13</sup>C-succinate were higher in the remote area of HMGCS2-rescued hearts compared with the infarct area (Figure 5R and Figure S14A and S14B). This indicates that the induction of CM glycolysis and aerobic glucose metabolism in the remote area would help to maintain their OCR and mitochondrial function, as mentioned previously for HMGCS2-overexpressing hearts (Figure 3H). At the same time, more H3P+ CMs were found at the border zone of HMGCS2-rescued hearts compared with control hearts (Figure 5S and 5T). In conclusion, cardiac ketogenesis leads to metabolic switching in adaptation to the hypoxic environment, thus supporting heart function and regeneration after injury (Figure 5U).

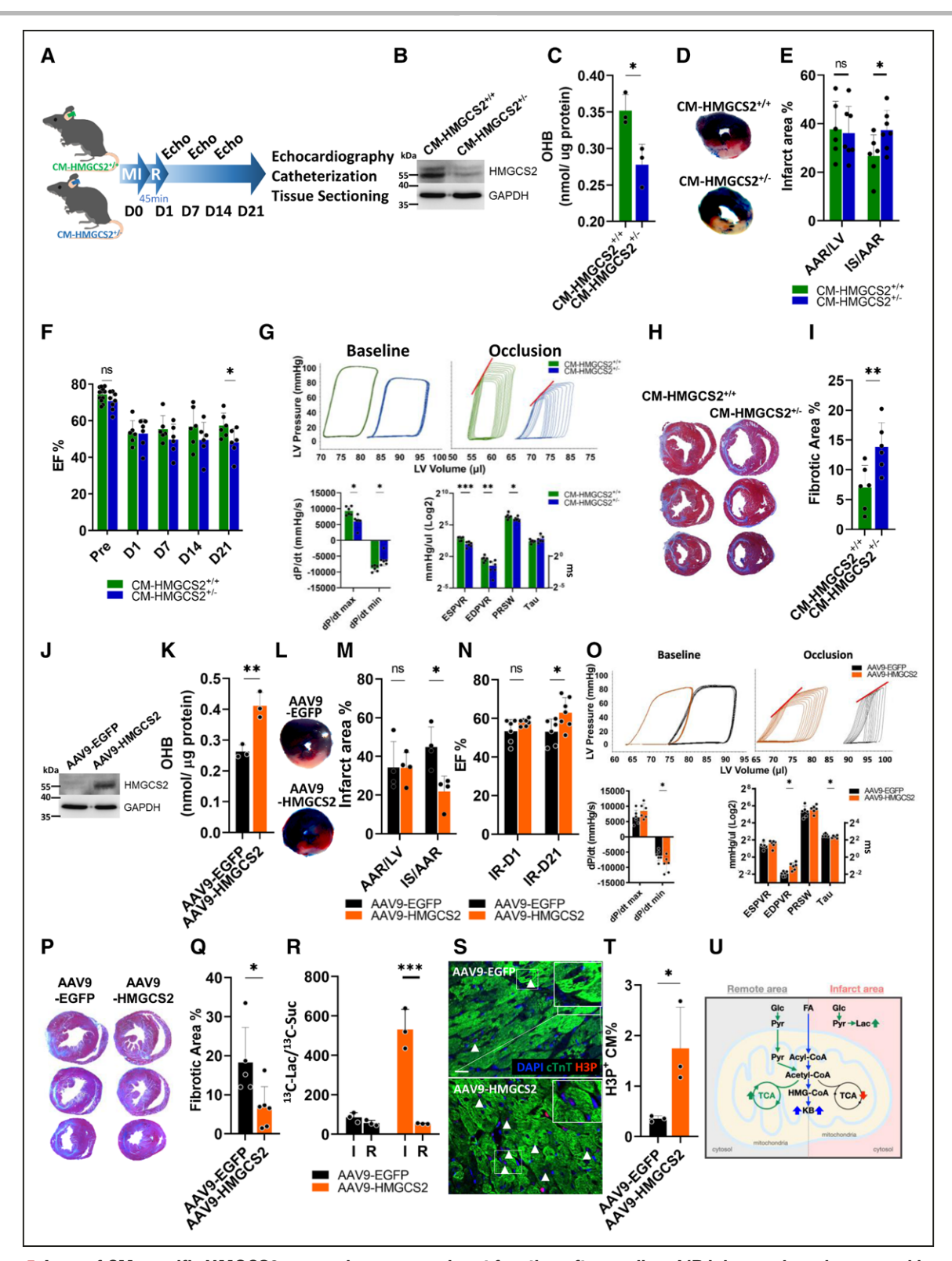


Figure 5. Loss of CM-specific HMGCS2 expression worsens heart function after cardiac cI/R injury and can be rescued by exogenous HMGCS2 expression.

A, Experimental design of cardiac ischemia/reperfusion (cI/R) on CM-HMGCS2+/- or CM-HMGCS2+/- mice. B, Protein expression of HMGCS2 measured by Western blot in cardiomyocytes (CMs) isolated from CM-HMGCS2+/- or CM-HMGCS2+/- mice after cl/R for 1 day. **C**, β-Hydroxybutyrate (OHB) level measured by OHB colorimetric assay in isolated CMs from CM-HMGCS2+/- or CM-HMGCS2+/- mice 1 day after cI/R. D, Infarct area presented by triphenyltetrazolium chloride (TTC) staining and remote area presented by Evans blue staining in heart sections of CM-HMGCS2+/+ or CM-HMGCS2+/- mice 1 day after cl/R. E, Quantification of infarct area percentage in heart sections of CM-HMGCS2+/+ or CM-HMGCS2+/- mice 1 day after cI/R. F, Ejection fraction percent (EF%) of CM-HMGCS2+/+ or (Continued)

Figure 5 Continued. CM-HMGCS2+/- hearts measured by echocardiography at different time points after cl/R. G, Heart function of CM-HMGCS2+/+ or CM-HMGCS2+/- mice determined by catheterization at post-cl/R day (D) 21. H, Fibrotic area in CM-HMGCS2+/+ or CM-HMGCS2+/- hearts shown by Masson trichrome staining of heart tissue sections at post-cl/R day 21. I, Quantification of fibrotic percentage in CM-HMGCS2+/+ or CM-HMGCS2+/- hearts at post-cl/R day 21 measured by Masson trichrome staining. J, Protein expression of HMGCS2 measured by Western blot in control or HMGCS2-rescued CM-HMGCS2+/- mice 1 day after cl/R. K, OHB level measured by OHB colorimetric assay in isolated CMs from control or HMGCS2-rescued CM-HMGCS2+/- mice 1 day after cI/R. L, Infarct area presented by TTC staining and remote area presented by Evans blue staining in heart sections of control or HMGCS2-rescued CM-HMGCS2+/- mice 1 day after cl/R. M, Quantification of infarct area percentage in heart sections of control or HMGCS2-rescued CM-HMGCS2+/- mice 1 day after cI/R. N, EF% of control or HMGCS2 rescued CM-HMGCS2+/- hearts measured by echocardiography at different time points after cl/R. 0, Heart function of control or HMGCS2-rescued CM-HMGCS2+/- hearts determined by catheterization at post-cI/R day 21. P, Fibrotic area in control or HMGCS2rescued CM-HMGCS2+/- hearts shown by Masson trichrome staining of heart tissue sections at post-cl/R day 21. **Q**, Quantification of fibrotic percentage in control or HMGCS2-rescued CM-HMGCS2+/- hearts at post-cl/R day 21 measured by Masson trichrome staining. R, Ratio of 13C-lactate to 13C-succinate in the infarct (I) or remote (R) areas measured by nuclear magnetic resonance through perfusing 13C-glucose with isolated hearts from control or HMGCS2-rescued CM-HMGCS2+/- mice at post-cl/R day 3. S, Immunofluorescence staining of heart tissue sections showing morphology of proliferative CMs through H3P and cardiac troponin T (cTnT) staining at the border zone of control or HMGCS2rescued CM-HMGCS2+/- mice at post-cl/R day 3. Arrowheads indicate H3P+/cTnT+ proliferative CMs. Scale bars are 50 μm. T, Quantification of proliferative CMs (H3P+ CM%) in the heart tissue sections of at the border zone of control or HMGCS2-rescued CM-HMGCS2+/- mice at postcI/R day 3. U, Schematic diagram of metabolic switch in the infarct and remote areas of control or HMGCS2-rescued CM-HMGCS2+/- hearts at post-cI/R day 3. AAR indicates area at risk; AAV9, adeno-associated virus serotype 9; EGFP, enhanced green fluorescent protein; IS, infarct size; and LV, left ventricular.

## Forced HMGCS2 Overexpression Increases Adult CM Dedifferentiation and Proliferation for Heart Function Improvement After MI or Under Hypoxia

Finally, we decided to investigate the possible therapeutic role of HMGCS2 on a permanent coronary artery ligation MI model (Figure 6A). After exogenous HMGCS2 induction by intramyocardial AAV9 injection immediately after MI, HMGCS2-overexpressing mice showed a higher EF% at post-MI day 21 than control AAV9-EGFP mice (Figure 6B). Catheter measurements indicated better heart function in HMGCS2-overexpressing mice 21 days after MI injury compared with control mice (Figure 6C). The infarct area showed no differences in control or HMGCS2-overexpressing mice 1 day after MI (Figure 6D and 6E), indicating that HMGCS2 overexpression may stimulate regeneration rather than protecting the myocardium. The fibrotic area was also smaller in HMGCS2-overexpressing mice compared with control mice (Figure 6F and 6G). More H3P+ CMs were found in HMGCS2-overexpressing hearts 3 days after MI injury compared with controls (Figure 6H and 6I). These proliferative CMs were all confirmed as HMGCS2+ (Figure S15A). Taken together, these findings show that exogenous HMGCS2 expression can support cardiac regeneration and improve heart function after MI.

Next, we decided to test these findings in a human system. We used an in vitro model using hypoxic (1%  $\rm O_2$ ) human iPSC-derived CMs (hiPSC-CMs; Figure 7A). HMGCS2 expression was highly upregulated in hiPSC-CMs after lentiviral infection (Lenti-HMGCS2) compared with control CMs (Lenti-EGFP; Figure 7B and Figure S15B). HMGCS2 overexpression also induces increased ketone production in hiPSC-CMs (Figure 7C). Furthermore, HMGCS2-overexpressing hiPSC-CMs showed a shorter morphology, with a lower length-to-width ratio compared with control cells under hypoxia

(Figure 7D-7G). HMGCS2-overexpressing hiPSC-CMs showed a 2-fold greater proliferative ability compared with control cells under hypoxic conditions, whereas the same proliferation induction could not be detected during normoxia (Figure 7H and Figure S15C). We further examined mitochondrial gene expression and morphology by real-time PCR and TEM, respectively. HMGCS2overexpressing iPSC-CMs showed lower mitochondrial RNA expression compared with controls (Figure 7I). In addition, the same poorly organized sarcomere structures with smaller, misaligned mitochondria were found in HMGCS2-overexpressing iPSC-CMs, whereas elongated mitochondria were aligned between sarcomeres in control cells (Figure 7J). These data indicate that forced HMGCS2 overexpression supports CM dedifferentiation and facilitates proliferation under hypoxic condition.

Furthermore, the mechanism by which HMGCS2 increases adult CM proliferation was examined. SRC has long been defined as an oncogene with the ability to increase cell proliferation, with its activation controlled by peroxisome proliferator-activated receptors (PPARs).23 HMGCS2 has also been reported to regulate transcriptional expression through association with  $\mbox{PPAR}\alpha.^{24}$  Thus, we hypothesized that HMGCS2 may activate Src expression to increase adult CM proliferation by associating with PPAR $\alpha$ . We found that both Ppar $\alpha$ and Src were significantly upregulated in HMGCS2overexpressing iPSC-CMs only under hypoxic conditions (Figure S16A). Downregulation of Src or Pparα expression was performed to test adult CM proliferation after HMGCS2 overexpression during hypoxia. Src downregulation by shRNA reduced expression to ≈10% (Figure S16B), and adult CMs showed 2 times lower proliferative ability than the control cells after culturing in a hypoxia chamber for 48 hours (Figure S16C). Downregulation of Pparα by shRNA was then performed in hiPSC-CMs during HMGCS2 overexpression, successfully reducing Ppar $\alpha$  expression to 20% (Figure S16D). Src expression

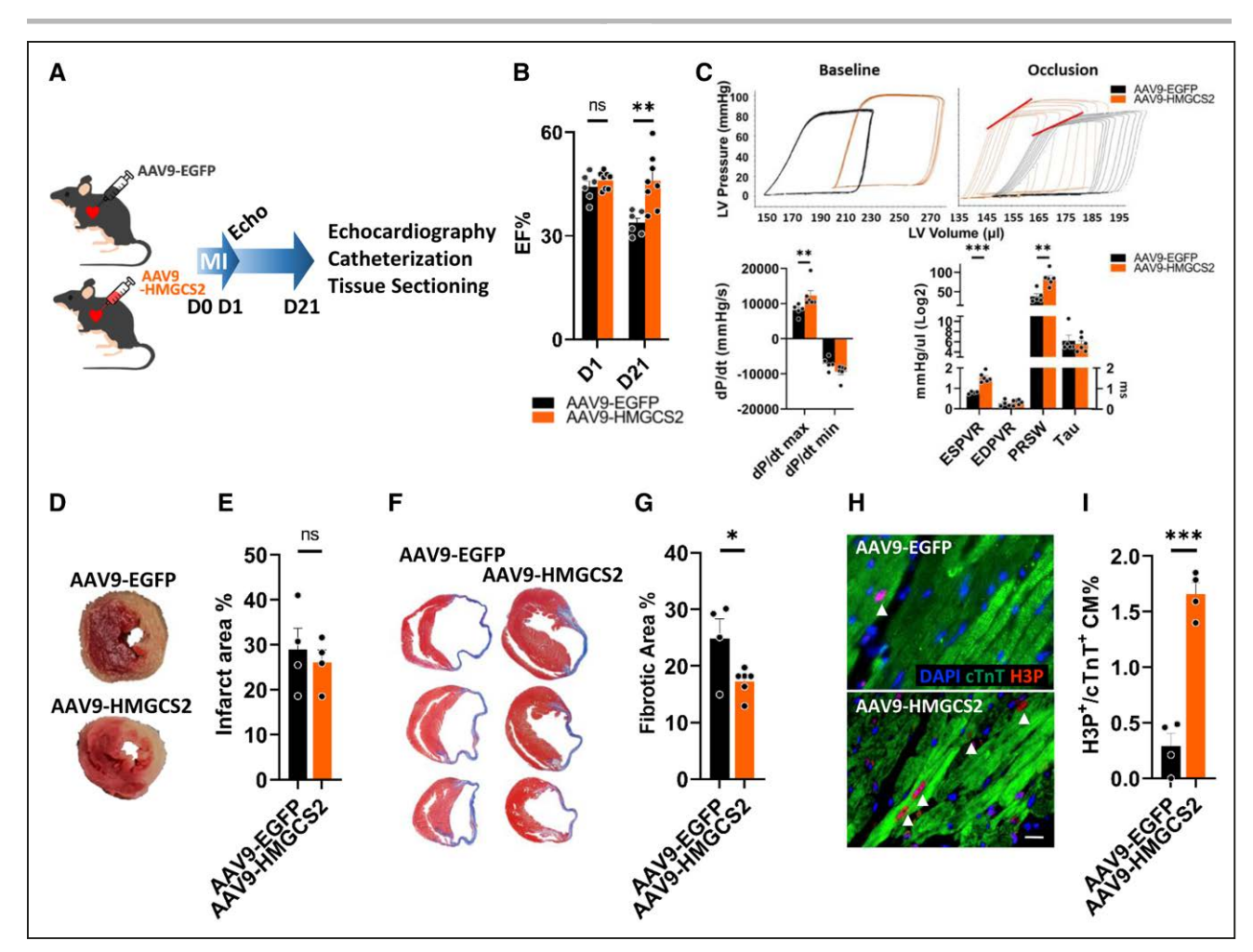
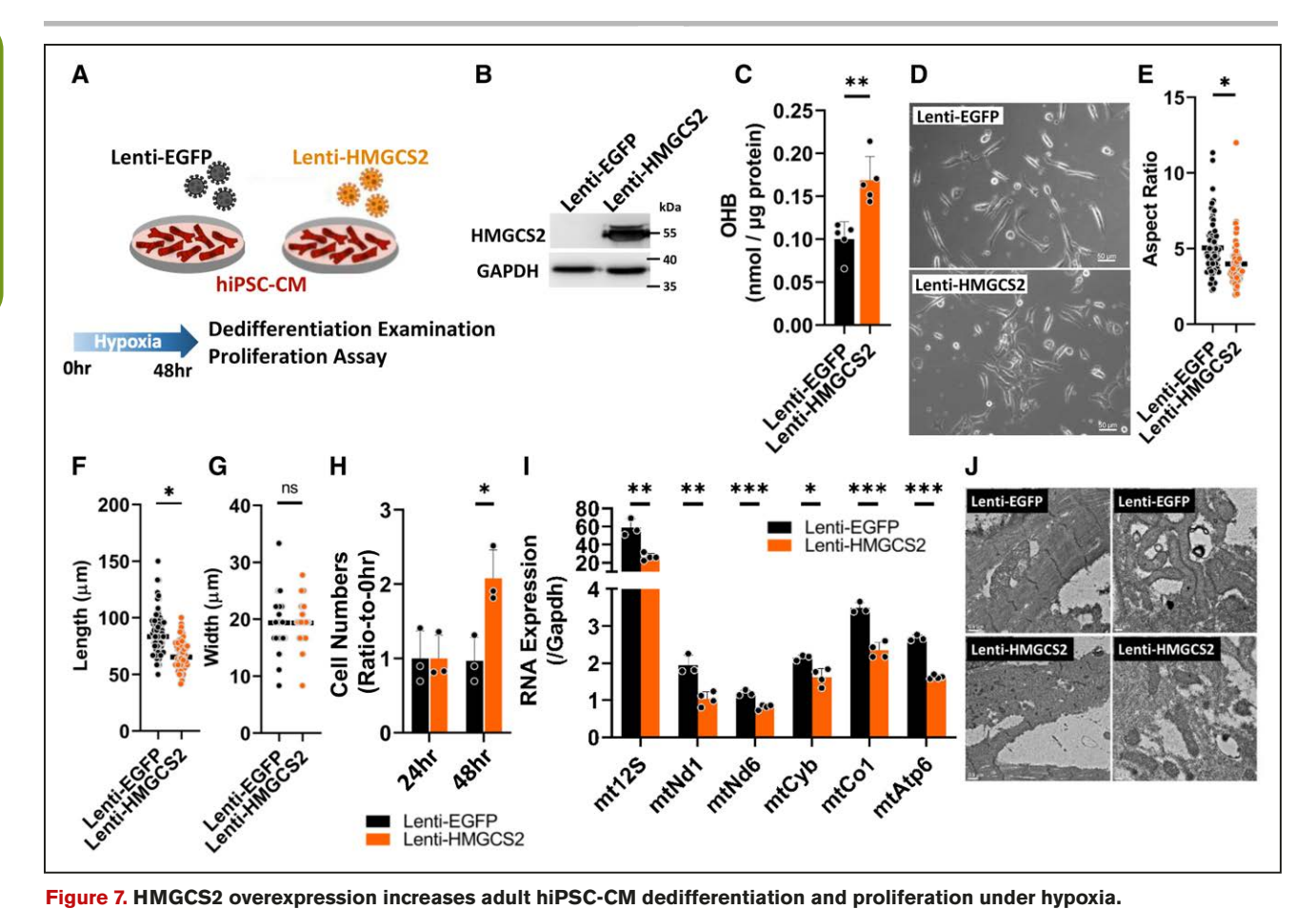


Figure 6. Forced HMGCS2 overexpression increases adult CM dedifferentiation and proliferation for heart function improvement after myocardial infarction.

A, Experimental design for performing myocardial infarction (MI) in adeno-associated virus serotype 9 (AAV9)-EGFP (enhanced green fluorescent protein) or AAV9-HMGCS2 mice. B, Heart function measured by echocardiography in AAV9-EGFP or AAV9-HMGCS2 mice. C, Heart function measured by catheterization in AAV9-EGFP or AAV9-HMGCS2 mice. D, Infarct area in AAV9-EGFP or AAV9-HMGCS2 hearts presented by triphenyltetrazolium chloride (TTC) staining of heart tissues at post-MI day 21. E, Quantification of infarct percentage in AAV9-EGFP or AAV9-HMGCS2 hearts at post-MI day 21 measured by TTC staining. F, Fibrotic area in AAV9-EGFP or AAV9-HMGCS2 hearts shown by Masson trichrome staining of heart tissue sections at post-MI day 21. G, Quantification of fibrotic percentage in AAV9-EGFP or AAV9-HMGCS2 hearts at post-MI day 21 measured by Masson trichrome staining. H, Immunofluorescence staining of heart tissue sections showing morphology of proliferative CMs through H3P and cardiac troponin T (cTnT) staining at the border zone of AAV9-EGFP or AAV9-HMGCS2 mice at post-MI day 3. Arrowheads indicate H3P+/cTnT+ proliferative CMs. Scale bars are 50 µm. I, Quantification of proliferative CMs (H3P+ CM%) in the heart tissue sections at the border zone of AAV9-EGFP or AAV9-HMGCS2 mice at post-MI day 3. EDPVR indicates end-diastolic pressurevolume relationship; ESPVR, end-systolic pressure-volume relationship; ns, not significant; and PRSW, preload recruitable stroke work.

was also found to be downregulated to ≈50% compared with control cells (Figure S16D). The proliferative ability was 1.6 times lower in Pparα knockdown cells than in control cells (Figure S16E). Pparα knockdown by the specific inhibitor GW6471 was also performed, and showed similar effects on reducing hiPSC-CM proliferation (Figure S16F and S16G). Furthermore, a mutant HMGCS2, unable to interact with PPARα, was generated. Palmitoylation of HMGCS2 has previously been reported to play an important role for its interaction with PPARα, and HMGCS2-C305S (mutant) could be generated to block this interaction without affecting its active site.25 Following the same strategy, HMGCS2-WT (wild type) or HMGCS2-C305S protein expression was con-

firmed to be upregulated in 293 cells after the induction of overexpression by lentivirus (Figure S16H). Immunoprecipitation results showed that strong interaction with PPARα was detected in HMGCS2-WT-overexpressing hiPSC-CMs, whereas the interaction was decreased in HMGCS2-C305S cells (Figure S16I). These data indicate that position 305 is essential for HMGCS2 interaction with PPARa. Furthermore, Src expression was downregulated in HMGCS2-C305S-overexpressing hiPSC-CMs compared with the WT cells (Figure S16J). Finally, the proliferative ability was significantly decreased in mutant HMGCS2-overexpressing cells compared with WT (Figure S16K). We further examined this mechanism in HMGCS2-overexpressing CM-OSKM hearts. Src



A, Experimental design for examining effects on forced HMGCS2 expression in human induced pluripotent stem cell-derived cardiomyocytes (hiPSC-CMs) after Lenti-EGFP (enhanced green fluorescent protein) or Lenti-HMGCS2 infection. B, Protein expression of HMGCS2 measured by Western blot in control or HMGCS2-overexpressed hiPSC-CMs under hypoxia. C, β-Hydroxybutyrate (OHB) level detected by OHB colorimetric assay in control or HMGCS2-overexpressed hiPSC-CMs under hypoxia. D, Morphology of control or HMGCS2-overexpressed hiPSC-CMs under hypoxia. E, Length of each control or HMGCS2-overexpressed hiPSC-CMs under hypoxia. E, Length of each control or HMGCS2-overexpressed hiPSC-CMs under hypoxia. H, Proliferative ability determined by length-to-width ratio of each control or HMGCS2-overexpressed hiPSC-CMs after culturing in hypoxia. H, Proliferative ability determined by calculation of CM numbers of control or HMGCS2-overexpressed hiPSC-CMs after culturing in hypoxia chamber for 48 hours. I, Mitochondrial RNA expression detected by real-time polymerase chain reaction in control or HMGCS2-overexpressed hiPSC-CMs after culturing in hypoxia chamber for 48 hours. These RNA expressions were normalized by Gapdh. J, Mitochondrial structure examined by transmission electron microscopy in control or HMGCS2-overexpressed hiPSC-CMs after culturing

expression was significantly upregulated only in reprogramming hearts compared with control hearts, while simultaneously inducing HMGCS2 overexpression (Figure S16L). We also investigated expression in the infarct border zone and remote area of hearts after HMGCS2 overexpression. Although Ppar $\alpha$  expression was high in both areas of the MI-performed hearts, and even higher in the remote area, Src expression was significantly upregulated only in the border zone area (Figure S16M). Taken together, these data indicate that HMGCS2 supports adult CM proliferation through association with PPAR $\alpha$  for inducing SRC expression.

## DISCUSSION

In a previous study, our group showed that in vitro reprogramming of neonatal mouse CMs upregulated expression of proliferation-related genes. We then delivered these genes to successfully drive CM proliferation through activation of the cell cycle. 18 However, neonatal CMs and adult CMs differ significantly in their structure, function, metabolism, and response to injury.26 As a result, the gene cocktail described in our previous study was unable to efficiently induce proliferation in adult CMs. Through specific induction of adult CM reprogramming in vivo, we not only can investigate the transformation of CMs during the process but also detect the effects on the whole mouse. The data presented here suggest that inducing a metabolic switch in adult CMs, rather than directly inducing cell cycle-related activators, may be a more efficient way to regain proliferative ability (Figures 1 and 2). A similar approach was published recently showing that short-term in vivo expression of OSKM in adult CMs induced dedifferentiation, enabling

in hypoxia chamber for 48 hours.

reentry into the cell cycle and facilitating heart regeneration.<sup>19</sup> Our 2 studies therefore clearly demonstrate that partial reprogramming is a potential tool in the regeneration toolkit. One notable difference is that our study used intraperitoneal doxycycline administration rather than oral (drinking water) administration. This evidently led to a different progression of CM reprogramming. In our study, CM proliferation peaked 2 days after doxycycline injection, and 6 days was lethal, with mice showing apoptotic CMs. However, the study by Chen et al showed a slower timeline of reprogramming, with dedifferentiation occurring at day 6.19 Extended administration of doxycycline resulted in cardiac tumors. Thus, it is clear that the reprogramming-based approach has limitations. Therefore, we were motivated to examine the adult CM reprogramming process and to identify any potentially modifiable downstream targets that may allow induction of temporary adult CM dedifferentiation. Our microarray analysis of CMs during early reprogramming revealed changes in genes associated with metabolism. We also note that the study by Chen et al found metabolism-related gene expression changes.<sup>19</sup> In the present study, we comprehensively profiled the metabolism of earlyreprogramming CMs using labeled substrates and identified a switch to ketogenesis.

Ketogenesis is carried out mainly in the liver, where ketones can be easily transferred to other tissues for use.<sup>27</sup> Ketone use is common as an alternative energy source during fasting or exercising,28 and ketones are used as a metabolic substrate in the heart after injury.<sup>29-31</sup> Under normal conditions with sufficient oxygen, the adult myocardium primarily uses FA and glucose oxidation, with ketone bodies used minimally for energy production.<sup>32</sup> However, if extra ketones are supplied, they can be used by the heart, subsequently reducing FA and glucose metabolism.<sup>33–35</sup> Failing hearts gradually lose their ability to oxidize FAs or glucose and alternatively use ketone oxidation to bypass the dysregulation of the β-oxidation pathway and pyruvate dehydrogenase complex. Despite mitochondrial damage during heart failure, ketones still can be completely oxidized with fewer steps.<sup>29,36</sup> Increased ketone use is thought to be adaptive because overexpression of the ketolysis enzyme BDH1 has been shown to attenuate cardiac remodeling in a pressure-overloaded model.<sup>30,37</sup> However, few studies have clearly defined the role of ketone synthesis in the heart tissue itself. Here, we provide evidence that HMGCS2-induced ketogenesis in adult CMs competitively reduces FA metabolism, leading to a metabolic switch and mitochondrial changes (Figures 2 and 3).

Metabolic flexibility allows cells to adapt to changing conditions and occurs primarily as a result of the antagonism between glucose and FA for providing energy production.<sup>38</sup> Several studies have demonstrated the importance of metabolic reprogramming in the heart during periods of stress. Decreased aerobic respiration has also been shown to provide a suitable environment for

adult CM proliferation by reduction of FA or glucose oxidation.<sup>39-41</sup> In a previous study, ectopic expression of cell cycle genes in hiPSC-CMs resulted in reduced oxidative phosphorylation and increased anabolic metabolism, including gluconeogenesis.40 Our study corroborates this because ketogenesis is also a form of anabolic metabolism and thus may create a favorable environment for increasing CM proliferation. In addition, ketogenesis regulates FA metabolism, glucose metabolism, and the tricarboxylic acid cycle for maintaining hepatic metabolic homeostasis.<sup>28,42,43</sup> The same scenario is presented in this study, showing that an increase of HMGCS2induced ketogenesis in adult CMs decreases FA metabolism. Glucose is then used through anaerobic or aerobic respiration, depending on the available oxygen. Thus, ketogenesis-induced adult CM reprogramming can be specifically induced in the border zone but not the remote area of injury hearts (Figure 5).

HMGCS2 is a rate-limiting enzyme for catalyzing the first reaction of ketogenesis.44 3-Hydroxy-3-methylglutaryl-CoA lyase deficiency is a rare autosomal recessive error of ketone body synthesis and leucine degradation. There are >20 different HMGCS2 mutations reported, and patients with these mutations have hepatomegaly and hypoglycemia during acute infection and prolonged fasting.45-49 HMGCS2 is upregulated in the mouse ventricle within 1 week after birth, and its expression is diminished at postnatal day 12.50 However, the role of HMGCS2 in the maintenance of heart function during development or after injury has not been previously investigated. In our study, we generated AAV9-HMGCS2 and CM-specific HMGCS2 knockout mice to thoroughly demonstrate the role of HMGCS2 in initiating adult CM dedifferentiation and proliferation, thus offering a degree of cardiac protection and regeneration after injury. Our study also provides other possible targets identified by microarray and metabolic profiling experiments, including upregulation of immune response and apoptosis-related genes and downregulation of nucleotide synthesis-related genes during early reprogramming. Each of these provides new research directions for future studies hoping to induce adult CM proliferation.

Overall, we have demonstrated the importance of HMGCS2-induced ketogenesis as a means to regulate metabolic response to CM injury, thus allowing cell dedifferentiation and proliferation as a regenerative response. Overlaps between OSKM-induced CM reprogramming, heart development and maturation, and the response to heart injury become readily apparent. Because MI remains the greatest cause of death in developed countries, we hope this study provides a foundation for future research exploiting metabolism as a mechanism to drive myocardial regeneration after injury.

#### ARTICLE INFORMATION

Received August 9, 2022; accepted September 29, 2022.

#### **Affiliations**

Institute of Biomedical Sciences (Y.-Y.C., R.P.P., T.-Y.M., Y.-H.H., Y.-C.L., S.-C.R., J.-H.L., P.-J.L., Y.-T.Y., P.C.H.H.) and Research Center for Applied Sciences (C.-W.K., P.C.), Academia Sinica, Taipei, Taiwan. Department of Medicine and Stem Cell and Regenerative Medicine Center, School of Medicine and Public Health, University of Wisconsin-Madison (Z.G., T.J.K., P.C.H.H.). Graduate Institute of Biomedical Materials and Tissue Engineering, Taipei Medical University, Taiwan (D.J.L.). Mitochondria and Metabolism Center, Department of Anesthesiology and Pain Medicine and Department of Bioengineering, University of Washington, Seattle (R.T.). Graduate Institute of Medical Genomics and Proteomics and Graduate Institute of Clinical Medicine, College of Medicine, National Taiwan University, Taipei (P.C.H.H.).

#### **Acknowledgments**

The authors are grateful to the Genomic Technology Core Laboratory at the Institute of Plant and Microbial Biology, Academia Sinica, for microarray analysis; the Metabolomics Core Laboratory at the Center of Genomic Medicine of National Taiwan University for Metabolomic experiments; and Academia Sinica High-Field NMR Center for technical support. The authors thank the Taiwan Mouse Clinic at Academia Sinica and Taiwan Animal Consortium for technical support in the seahorse analysis. The authors thank the National RNAi Core Facility at Academia Sinica in Taiwan for providing shRNA reagents and related services. FACS, high-content imaging, and animal studies were supported by Core Facility located at the Institute of Biomedical Sciences, and TEM imaging was supported by Core Facility located at the Institute of Cellular and Organismic Biology, Academia Sinica. Y.-Y.C. and P.C.H.H. conceived the original idea and discussed with T.J.K. and Z.G. to eventually conclude the main focus of this study. Y.-Y.C. designed and performed the experiments and wrote the manuscript. Z.G. edited the manuscript. R.P.P. performed the whole NMR and high-performance liquid chromatography experiments. D.J.L. helped with experimental design, study guidance and manuscript writing. T.-Y.M., Y.-H.H., and Y.-C.L. performed the study experiments. S.-C.R., J.-H.L., and P.-J.L. performed animal surgeries and measurements. C.-W.K. and P.C. performed intravital microscopy. Y.-T.Y. and R.T. supervised the whole study. T.J.K. and P.C.H.H. supervised and managed the study.

#### Sources of Funding

The High-Field NMR Center is funded by Academia Sinica Core Facility and Innovative Instrument Project (AS-CFII-108-112). This work was supported by the Ministry of Science and Technology, Taiwan (109-2321-B-001-012, 109-2327-B-001-001, 109-2740-B-001-002), the National Health Research Institutes (EX109-10907SI), the Academia Sinica Thematic Research Program (AS-107-TPL12), the Healthy Longevity Grand Challenge (AS-HLGC-109-05), the Translational Medical Research Program (AS-KPQ-110-BioMed), and the University of Wisconsin Institute for Clinical and Translational Research (UL1TR002373 from the National Institutes of Health/National Center for Advancing Translational Sciences).

#### **Disclosures**

None.

#### **Supplemental Material**

Figures S1–S16 Tables S1-S2 Expanded Methods References 51–56

## **REFERENCES**

- Kubin T, Poling J, Kostin S, Gajawada P, Hein S, Rees W, Wietelmann A, Tanaka M, Lorchner H, Schimanski S, et al. Oncostatin M is a major mediator of cardiomyocyte dedifferentiation and remodeling. *Cell Stem Cell*. 2011;9:420–432. doi: 10.1016/j.stem.2011.08.013
- Jopling C, Sleep E, Raya M, Marti M, Raya A, Izpisua Belmonte JC. Zebrafish heart regeneration occurs by cardiomyocyte dedifferentiation and proliferation. *Nature*. 2010;464:606–609. doi: 10.1038/nature08899
- 3. Gupta V, Poss KD. Clonally dominant cardiomyocytes direct heart morphogenesis. *Nature*. 2012;484:479–484. doi: 10.1038/nature11045
- Sturzu AC, Rajarajan K, Passer D, Plonowska K, Riley A, Tan TC, Sharma A, Xu AF, Engels MC, Feistritzer R, et al. Fetal mammalian heart generates a robust compensatory response to cell loss. *Circulation*. 2015;132:109– 121. doi: 10.1161/CIRCULATIONAHA.114.011490
- Sereti KI, Nguyen NB, Kamran P, Zhao P, Ranjbarvaziri S, Park S, Sabri S, Engel JL, Sung K, Kulkarni RP, et al. Analysis of cardiomyocyte clonal expansion during mouse heart development and injury. *Nat Commun.* 2018;9:754. doi: 10.1038/s41467-018-02891-z

- Bersell K, Arab S, Haring B, Kuhn B. Neuregulin1/ErbB4 signaling induces cardiomyocyte proliferation and repair of heart injury. *Cell.* 2009; 138:257–270. doi: 10.1016/j.cell.2009.04.060
- 7. Hsieh PCH, Kamp TJ. To be young at heart. *Cell Stem Cell*. 2018;22:475–476. doi: 10.1016/j.stem.2018.03.003
- Mohamed TMA, Ang YS, Radzinsky E, Zhou P, Huang Y, Elfenbein A, Foley A, Magnitsky S, Srivastava D. Regulation of cell cycle to stimulate adult cardiomyocyte proliferation and cardiac regeneration. *Cell.* 2018;173:104– 116.e12. doi: 10.1016/j.cell.2018.02.014
- Liu S, Li K, Wagner Florencio L, Tang L, Heallen TR, Leach JP, Wang Y, Grisanti F, Willerson JT, Perin EC, et al. Gene therapy knockdown of Hippo signaling induces cardiomyocyte renewal in pigs after myocardial infarction. Sci Transl Med. 2021;13:eabd6892. doi: 10.1126/scitranslmed. abd6892
- Ahuja P, Perriard E, Perriard JC, Ehler E. Sequential myofibrillar breakdown accompanies mitotic division of mammalian cardiomyocytes. *J Cell Sci.* 2004;117:3295–3306. doi: 10.1242/jcs.01159
- Lepilina A, Coon AN, Kikuchi K, Holdway JE, Roberts RW, Burns CG, Poss KD. A dynamic epicardial injury response supports progenitor cell activity during zebrafish heart regeneration. *Cell.* 2006;127:607–619. doi: 10.1016/j.cell.2006.08.052
- Kikuchi K, Holdway JE, Werdich AA, Anderson RM, Fang Y, Egnaczyk GF, Evans T, Macrae CA, Stainier DY, Poss KD. Primary contribution to zebrafish heart regeneration by gata4(+) cardiomyocytes. *Nature*. 2010;464:601– 605. doi: 10.1038/nature08804
- Karwi QG, Uddin GM, Ho KL, Lopaschuk GD. Loss of metabolic flexibility in the failing heart. Front Cardiovasc Med. 2018;5:68. doi: 10.3389/fcvm. 2018.00068
- Bergmann O, Zdunek S, Felker A, Salehpour M, Alkass K, Bernard S, Sjostrom SL, Szewczykowska M, Jackowska T, Dos Remedios C, et al. Dynamics of cell generation and turnover in the human heart. *Cell*. 2015;161:1566-1575. doi: 10.1016/j.cell.2015.05.026
- Neubauer S. The failing heart: an engine out of fuel. N Engl J Med. 2007;356:1140-1151. doi: 10.1056/NEJMra063052
- Takahashi K, Yamanaka S. Induction of pluripotent stem cells from mouse embryonic and adult fibroblast cultures by defined factors. *Cell*. 2006;126:663–676. doi: 10.1016/j.cell.2006.07.024
- Wu J, Ocampo A, Belmonte JCI. Cellular metabolism and induced pluripotency. Cell. 2016;166:1371–1385. doi: 10.1016/j.cell.2016.08.008
- Cheng YY, Yan YT, Lundy DJ, Lo AH, Wang YP, Ruan SC, Lin PJ, Hsieh PC. Reprogramming-derived gene cocktail increases cardiomyocyte proliferation for heart regeneration. *EMBO Mol Med.* 2017;9:251–264. doi: 10.15252/emmm.201606558
- Chen Y, Luttmann FF, Schoger E, Scholer HR, Zelarayan LC, Kim KP, Haigh JJ, Kim J, Braun T. Reversible reprogramming of cardiomyocytes to a fetal state drives heart regeneration in mice. *Science*. 2021;373:1537– 1540. doi: 10.1126/science.abg5159
- Li T, Zhang Z, Kolwicz SC Jr, Abell L, Roe ND, Kim M, Zhou B, Cao Y, Ritterhoff J, Gu H, et al. Defective branched-chain amino acid catabolism disrupts glucose metabolism and sensitizes the heart to ischemia-reperfusion injury. Cell Metab. 2017;25:374–385. doi: 10.1016/j.cmet.2016.11.005
- Marsboom G, Toth PT, Ryan JJ, Hong Z, Wu X, Fang YH, Thenappan T, Piao L, Zhang HJ, Pogoriler J, et al. Dynamin-related protein 1-mediated mitochondrial mitotic fission permits hyperproliferation of vascular smooth muscle cells and offers a novel therapeutic target in pulmonary hypertension. *Circ Res.* 2012;110:1484–1497. doi: 10.1161/ circresaha.111.263848
- Camarero N, Mascaro C, Mayordomo C, Vilardell F, Haro D, Marrero PF. Ketogenic HMGCS2 is a c-Myc target gene expressed in differentiated cells of human colonic epithelium and down-regulated in colon cancer. *Mol Cancer Res.* 2006;4:645–653. doi: 10.1158/1541-7786.MCR-05-0267
- Montagner A, Delgado MB, Tallichet-Blanc C, Chan JS, Sng MK, Mottaz H, Degueurce G, Lippi Y, Moret C, Baruchet M, et al. Src is activated by the nuclear receptor peroxisome proliferator-activated receptor beta/delta in ultraviolet radiation-induced skin cancer. *EMBO Mol Med*. 2014;6:80–98. doi: 10.1002/emmm.201302666
- Meertens LM, Miyata KS, Cechetto JD, Rachubinski RA, Capone JP. A mitochondrial ketogenic enzyme regulates its gene expression by association with the nuclear hormone receptor PPARalpha. EMBO J. 1998; 17:6972-6978. doi: 10.1093/emboj/17.23.6972
- Kostiuk MA KB, Berthiaume LG. Palmitoylation of ketogenic enzyme HMGCS2 enhances its interaction with PPARalpha and transcription at the Hmgcs2 PPRE. FASEB J. 2010;24:1914–1924. doi: 10.1096/fj. 09-149765

- 26. Szibor M, Poling J, Warnecke H, Kubin T, Braun T. Remodeling and dedifferentiation of adult cardiomyocytes during disease and regeneration. Cell Mol Life Sci. 2014;71:1907-1916. doi: 10.1007/s00018-013-1535-6
- 27. Grabacka M, Pierzchalska M, Dean M, Reiss K. Regulation of ketone body metabolism and the role of PPARalpha. Int J Mol Sci . 2016; 17:2093. doi: 10.3390/ijms17122093
- 28. Puchalska P, Crawford PA. Multi-dimensional roles of ketone bodies in fuel metabolism, signaling, and therapeutics. Cell Metab. 2017;25:262-284. doi: 10.1016/j.cmet.2016.12.022
- 29. Aubert G, Martin OJ, Horton JL, Lai L, Vega RB, Leone TC, Koves T, Gardell SJ, Kruger M, Hoppel CL, et al. The failing heart relies on ketone bodies as a fuel. Circulation. 2016;133:698-705. doi: 10.1161/ CIRCULATIONAHA.115.017355
- 30. Horton JL, Davidson MT, Kurishima C, Vega RB, Powers JC, Matsuura TR, Petucci C, Lewandowski ED, Crawford PA, Muoio DM, et al. The failing heart utilizes 3-hydroxybutyrate as a metabolic stress defense. JCI Insight. 2019;4:e124079. doi: 10.1172/jci.insight.124079
- 31. Nielsen R, Moller N, Gormsen LC, Tolbod LP, Hansson NH, Sorensen J, Harms HJ. Frokiaer J. Eiskiaer H. Jespersen NR. et al. Cardiovascular effects of treatment with the ketone body 3-hydroxybutyrate in chronic heart failure patients. Circulation. 2019;139:2129-2141. doi: 10.1161/ CIRCULATIONAHA.118.036459
- 32. Ho KL, Zhang L, Wagg C, Al Batran R, Gopal K, Levasseur J, Leone T, Dyck JRB, Ussher JR, Muoio DM, et al. Increased ketone body oxidation provides additional energy for the failing heart without improving cardiac efficiency. Cardiovasc Res. 2019;115:1606-1616. doi: 10.1093/cvr/cvz045
- 33. Bassenge E, Wendt VE, Schollmeyer P, Bluemchen G, Gudbjarnason S, Bing RJ. Effect of ketone bodies on cardiac metabolism, Am J Physiol, 1965;208:162-168. doi: 10.1152/ajplegacy.1965.208.1.162
- 34. Stanley WC, Meadows SR, Kivilo KM, Roth BA, Lopaschuk GD. Betahydroxybutyrate inhibits myocardial fatty acid oxidation in vivo independent of changes in malonyl-CoA content. Am J Physiol Heart Circ Physiol. 2003;285:H1626-H1631. doi: 10.1152/ajpheart.00332.2003
- 35. Ziegler A, Zaugg CE, Buser PT, Seelig J, Kunnecke B. Non-invasive measurements of myocardial carbon metabolism using in vivo 13C NMR spectroscopy. NMR Biomed. 2002;15:222-234. doi: 10.1002/nbm.764
- Bedi KC Jr, Snyder NW, Brandimarto J, Aziz M, Mesaros C, Worth AJ, Wang LL, Javaheri A, Blair IA, Margulies KB, et al. Evidence for intramyocardial disruption of lipid metabolism and increased myocardial ketone utilization in advanced human heart failure. Circulation. 2016;133:706-716. doi: 10.1161/CIRCULATIONAHA.115.017545
- 37. Uchihashi M, Hoshino A, Okawa Y, Ariyoshi M, Kaimoto S, Tateishi S, Ono K, Yamanaka R, Hato D, Fushimura Y, et al. Cardiac-specific Bdh1 overexpression ameliorates oxidative stress and cardiac remodeling in pressure overload-induced heart failure. Circ Heart Fail. 2017;10:e004417. doi: 10.1161/CIRCHEARTFAILURE.117.004417
- 38. Goodpaster BH, Sparks LM. Metabolic flexibility in health and disease. Cell Metab. 2017;25:1027-1036. doi: 10.1016/j.cmet.2017.04.015
- 39. Cardoso AC, Lam NT, Savla JJ, Nakada Y, Pereira AHM, Elnwasany A, Menendez-Montes I, Ensley EL, Petric UB, Sharma G, et al. Mitochondrial substrate utilization regulates cardiomyocyte cell cycle progression. Nat Metab. 2020;2:167-178.
- 40. Bae J, Salamon RJ, Brandt EB, Paltzer WG, Zhang Z, Britt EC, Hacker TA, Fan J, Mahmoud Al. Malonate promotes adult cardiomyocyte proliferation and heart regeneration. Circulation. 2021;143:1973-1986. doi: 10.1161/CIRCULATIONAHA.120.049952
- 41. Abouleisa RRE, McNally L, Salama ABM, Hammad SK, Ou O, Wells C, Lorkiewicz PK, Bolli R, Mohamed TMA, Hill BG. Cell cycle induction in human cardiomyocytes is dependent on biosynthetic pathway activation. Redox Biol. 2021;46:102094. doi: 10.1016/j.redox.2021.102094

- 42. Cotter DG, Ercal B, Huang X, Leid JM, d'Avignon DA, Graham MJ, Dietzen DJ, Brunt EM, Patti GJ, Crawford PA. Ketogenesis prevents dietinduced fatty liver injury and hyperglycemia. J Clin Invest. 2014;124: 5175-5190. doi: 10.1172/JCI76388
- 43. Arima Y, Nakagawa Y, Takeo T, Ishida T, Yamada T, Hino S, Nakao M, Hanada S. Umemoto T. Suda T. et al. Murine neonatal ketogenesis preserves mitochondrial energetics by preventing protein hyperacetylation. Nat Metab. 2021;3:196-210. doi: 10.1038/s42255-021-00342-6

ORIGINAL RESEARCH

- 44. Hegardt FG. Mitochondrial 3-hydroxy-3-methylglutaryl-CoA synthase: a control enzyme in ketogenesis. Biochem J. 1999;338:569-582. doi: 10.1042/bj3380569
- 45. Thompson GN, Hsu BY, Pitt JJ, Treacy E, Stanley CA. Fasting hypoketotic coma in a child with deficiency of mitochondrial 3-hydroxy-3-methylglutaryl-CoA synthase. N Engl J Med. 1997;337:1203-1207. doi: 10.1056/NEJM199710233371704
- Wolf NI, Rahman S, Clayton PT, Zschocke J. Mitochondrial HMG-CoA synthase deficiency: identification of two further patients carrying two novel mutations. Eur J Pediatr. 2003;162:279-280. doi: 10.1007/s00431-002-1110-x
- 47. Pitt JJ, Peters H, Boneh A, Yaplito-Lee J, Wieser S, Hinderhofer K, Johnson D, Zschocke J. Mitochondrial 3-hydroxy-3-methylglutaryl-CoA synthase deficiency: urinary organic acid profiles and expanded spectrum of mutations. J Inherit Metab Dis. 2015;38:459-466. doi: 10.1007/s10545-014-9801-9
- 48. Puisac B, Marcos-Alcalde I, Hernandez-Marcos M, Tobajas Morlana P, Levtova A, Schwahn BC, DeLaet C, Lace B, Gomez-Puertas P, Pie J. Human mitochondrial HMG-CoA synthase deficiency: role of enzyme dimerization surface and characterization of three new patients. Int J Mol Sci. 2018:19:1010. doi: 10.3390/iims19041010
- 49. Ramos M, Menao S, Arnedo M, Puisac B, Gil-Rodriguez MC, Teresa-Rodrigo ME, Hernandez-Marcos M, Pierre G, Ramaswami U, Baquero-Montoya C, et al. New case of mitochondrial HMG-CoA synthase deficiency: functional analysis of eight mutations. Eur J Med Genet. 2013;56:411-415. doi: 10.1016/j.ejmg.2013.05.008
- 50. Talman V, Teppo J, Poho P, Movahedi P, Vaikkinen A, Karhu ST, Trost K, Suvitaival T, Heikkonen J, Pahikkala T, et al. Molecular atlas of postnatal mouse heart development. J Am Heart Assoc. 2018;7:e010378. doi: 10.1161/JAHA.118.010378
- 51. Stadtfeld M, Maherali N, Borkent M, Hochedlinger K. A reprogrammable mouse strain from gene-targeted embryonic stem cells. Nat Methods. 2010;7:53-55. doi: 10.1038/nmeth.1409
- 52. Vinegoni C, Aguirre AD, Lee S, Weissleder R. Imaging the beating heart in the mouse using intravital microscopy techniques. Nat Protoc. 2015; 10:1802-1819. doi: 10.1038/nprot.2015.119
- Wang SY, Kuo CH, Tseng YJ. Ion trace detection algorithm to extract pure ion chromatograms to improve untargeted peak detection quality for liquid chromatography/time-of-flight mass spectrometry-based metabolomics data. Anal Chem. 2015;87:3048-3055. doi: 10.1021/ac504711d
- 54. van der Heijden R, de Boer-Hlupá V, Verpoorte R, Duine JA. Enzymes involved in the metabolism of 3-hydroxy-3-methylglutaryl-coenzyme A in Catharanthus roseus. Plant Cell Tissue Organ Cult. 1994;38:345-349. doi: 10.1007/bf00033895
- 55. Karamanlidis G, Lee CF, Garcia-Menendez L, Kolwicz SC Jr, Suthammarak W, Gong G, Sedensky MM, Morgan PG, Wang W, Tian R. Mitochondrial complex I deficiency increases protein acetylation and accelerates heart failure. Cell Metab. 2013;18:239-250. doi: 10.1016/j.cmet. 2013.07.002
- 56. Bohl S, Medway DJ, Schulz-Menger J, Schneider JE, Neubauer S, Lygate CA. Refined approach for quantification of in vivo ischemia-reperfusion injury in the mouse heart. Am J Physiol Heart Circ Physiol. 2009; 297:H2054-H2058. doi: 10.1152/ajpheart.00836.2009